Orthros: A Low-Latency PRF*

Subhadeep Banik[1] and Takanori Isobe[2,3,4] and
Fukang Liu[2,5] and Kazuhiko Minematsu[6] and Kosei Sakamoto[2]

[1] LASEC, École Polytechnique Fédérale de Lausanne, Switzerland.
subhadeep.banik@epfl.ch
[2] University of Hyogo, Kobe, Japan. takanori.isobe@ai.u-hyogo.ac.jp,
liufukangs@gmail.com, k.sakamoto0728@gmail.com
[3] NICT, Tokyo, Japan
[4] PRESTO, Japan Science and Technology Agency, Tokyo, Japan
[5] East China Normal University, Shanghai, China
[6] NEC, Kawasaki, Japan k-minematsu@nec.com

Abstract. We present Orthros, a 128-bit block pseudorandom function. It is designed with primary focus on latency of fully unrolled circuits. For this purpose, we adopt a parallel structure comprising two keyed permutations. The round function of each permutation is similar to Midori, a low-energy block cipher, however we thoroughly revise it to reduce latency, and introduce different rounds to significantly improve cryptographic strength in a small number of rounds. We provide a comprehensive, dedicated security analysis. For hardware implementation, Orthros achieves the lowest latency among the state-of-the-art low-latency primitives. For example, using the STM 90nm library, Orthros achieves a minimum latency of around 2.4 ns, while other constructions like PRINCE, Midori-128 and QARMA$_9$-128-σ_0 achieve 2.56 ns, 4.10 ns, 4.38 ns respectively.

Keywords: Pseudorandom Function, Low Latency, Lightweight Cryptography, Sum of Permutations

1 Introduction

1.1 Low-Latency Encryption

Lightweight cryptography is a subfield of symmetric-key cryptography to study cryptographic core functions usable under strong resource constraints. Hardware circuit size is a typical metric, and there are numerous proposals such as GIFT [BPP$^+$17], KATAN [DDK09], LED [GPPR11], Piccolo [SIH$^+$11], PRESENT [BKL$^+$07], and SIMON [BSS$^+$13] particularly perform well on this metric. Some other metrics exist, and among them, latency has been increasingly receiving attention. Latency affects the response time of encryption or authentication, and a small latency is highly desirable for applications that require instant response, such

[*] This is the revised version of the paper published from ToSC 2021 issue 1 [BIL$^+$21]. We revised some typos in the formula of the S-box in Sect. 3.3. Other contents are the same as the original version.

as encryption of memory bus, storage systems, automotive communication and industrial control network. Gaining throughput is generally possible with common signal processing techniques (pipelining and parallel processing), while achieving a low latency remains a challenge [KNR12].

To our knowledge, the first lightweight block cipher with explicit focus on latency is PRINCE proposed by Borghoff *et al.* [BCG$^+$12]. PRINCE is a 64-bit block cipher comprising multiple round functions to significantly reduce the number of rounds while keeping a moderate complexity of each round. Another proposal is QARMA proposed by Avanzi [Ava17], which is a family of low-latency tweakable block ciphers (TBCs) [LRW02]. It adopts the design strategy of PRINCE. Mantis [BJK$^+$16] is another family of low-latency TBCs. Midori is a family of block ciphers proposed by Banik *et al.* [BBI$^+$15]. It primary aims to reduce energy, however its latency is also quite small.

The current work on low-latency encryption focused on invertible primitives, *i.e.*, (tweakable) block ciphers. We started with a question whether this is an exclusive approach – namely, whether we can do better by not requiring an invertible primitive. Motivated by this question, we initiated a study on designing low-latency (non-invertible) pseudorandom function (PRF) consisting of parallel keyed permutations. We study a sum of two block ciphers denoted as $C = E_K(M) \oplus E'_K(M)$, where $E, E' : \mathcal{K} \times \mathcal{M} \to \mathcal{M}$ are different n-bit block ciphers with a key space $\mathcal{K}$ and a message space $\mathcal{M} = \{0,1\}^n$. Since E and E' can be computed in parallel, the critical path length of a fully unrolled circuit is a maximum of them instead of the sum. The resulting function has n-bit block and is not invertible in general.

The sum of permutations is indeed not new and it has been adopted in the designs of RIPEMD-160 [DBP96] and Grøstl [GKM$^+$09]. In addition, the sum of permutations has also been extensively studied in the context of provable security (see Section 3.1). In particular, the result of Dai *et al.* [DHT17] suggests that it can ideally achieve n-bit PRF security, *i.e.*, indistinguishable from a truly random function with $O(2^n)$ complexity. However this requires that E_K and E'_K behave as computationally-secure block ciphers, more formally, (computationally-)independent *pseudorandom permutations (PRPs).* Instead of requiring this, we explore the setting that E and E' are rather weak as a stand-alone block cipher, using a small number of very simple rounds. The point is that the outputs of E and E' are never given in clear, hence we can hope that both can cover each weakness, and consequently the sum of them can tolerate dedicated attacks as a PRF.

1.2 Our Design

Based on the aforementioned considerations, we present Orthros, which is a 128-bit block pseudorandom function (PRF) with a 128-bit key. The overall structure of Orthros is a sum of two SPN-type keyed permutations called Branch1 and Branch2. The round functions of Orthros are based on Midori. It is already suitable to low-latency ciphers, however we performed a thorough study on it and showed that we can further improve latency by adopting new permutation layers and S-boxes.

In particular, we propose a hybrid use of bit and nibble permutations *i.e.*, a bit permutation is used for some rounds and a nibble permutation for the rest, while Midori-128 [BBI$^+$15] uses a single linear layer including both of a bit permutation and a nibble permutation. Consequently, each branch of Orthros achieves the 2.5-round full diffusion and attains 64 active S-boxes over 10 rounds, while Midori-128 requires 3 rounds for the full diffusion and 13 rounds for 64 active S-boxes. In addition, the whole Orthros has more than 64 active S-boxes over only 5 rounds. Importantly, this change of linear layers does not require any additional hardware cost in an unrolled implementation.

For PRF, we do not need an involutory S-box unlike Midori and QARMA. This allows us to develop a new 4-bit S-box that offers about twice smaller delay than that of Midori-128 [BBI$^+$15] (see Table 8 of Page 14).

Since we do not rely on provable security of Sum of Permutations, we carried out an extensive security analysis on not only the components of Branch1 and Branch2 but also the whole Orthros.

Motivation for using 128-bit PRF. The lack of invertibility limits applications. For example the classical CBC and XTS (a storage encryption mode) [Dwo10] require the decryption routine of a block cipher. However, many popular modes, *e.g.*, CTR, CMAC [Dwo05] and GCM [NIS07], do not require the decryption routine (this property is also called inverse-freeness). For these modes Orthros can be used as the cryptographic core. For examples of applications that require low latency, ARM's pointer authentication code (PAC) uses QARMA [Qua]. PAC is a MAC for the pointer value and the memory context and it is derived by truncating the output of QARMA in an ECB-like mode. The length of PAC ranges from 11 to 31 bits or 3 to 23 bits, depending on a processor feature [Qua]. The PAC is inserted into a reserved space of the original 64-bit pointer containing the address. This mode is inverse-free, even though QARMA is an invertible primitive.

As another example we consider memory protection schemes based on (a MAC variant of) Merkle Tree. They often use a black-box PRF as a MAC function (*e.g.*, [HJ06]), and a concrete memory encryption scheme inside Intel's SGX [Gue16] adopts inverse-free modes, namely variants of GMAC and GCM. A notable benefit of using a dedicated PRF instead of a PRP is that it can provide a stronger, beyond-birthday-bound (BBB) security depending on the mode. As observed by [MN17b], by changing the component of GCM or CTR from a PRP to a PRF, the provable security immediately improves from $n/2$ to n bits. In such a case, there is a strong incentive to use a PRF from the security perspective.

If we compare our proposal with PRINCE, the larger input and output extend possible applications. In fact, the first example of PAC requires input larger than 64 bits while not exceeding 128 bits. This excludes the application of PRINCE [Qua, Page 6 (Cryptography)] and makes Orthros usable. In the latter example of tree-based memory protection, a GCM-like authenticated encryption mode with PRINCE will only have 32-bit security while Orthros ensures 128-bit security as described above. We note that the output size is also crucial for

128-bit security in this case, since we need 128 bits of pseudorandom sequence to mask 128-bit universal hash function output.

Implementations. We implemented Orthros in four different standard cell libraries along with 2 other constructions Midori-128 and QARMA$_9$-128-σ_0 that have a block size of 128 bits and offer at least 128 bits of security. Across all libraries, Orthros performs around 40 % better than the above designs with respect to **a)** the absolute delay between input/output ports and also **b)** the delay when the circuits are restricted to a certain area/power budget. We even found that Orthros performs marginally better than PRINCE (which has a blocksize of 64 bits and offers (127 - d) bits of security give 2^d plaintext /ciphertext pairs) with respect to the total circuit delay across all libraries. All our implementations are publicly available[7].

Related Work. Mennink and Neves [MN17b] proposed a generalized EDMD mode [MN17a] and an instantiation of it by a pair of reduced-round block ciphers, E and E'. The resulting scheme is a PRF of nearly n-bit security [MN17a] if E and E' are PRPs. In [MN17b] they proposed an instantiation based on reduced-round AES, called AES-PRF. It has been analyzed by Derbez *et al.* [DIS$^+$18]. Although a conceptual similarity to us, the generalized EDMD is not suitable for low-latency PRF because it is serial. Besides, they did not consider to use dedicated round functions. In a broader context, reduced-round version of a standard block cipher has been used to build a wide variety of cryptographic functions. Most notably for AES, there are examples such as a MAC function [DR05b, DR05a], a stream cipher [Bir07], a hash function [GM16], an authenticated encryption scheme [HKR15], and a tweakable block cipher [BGGS20] to name a few.

From the provable security perspective, the n-bit security of sum of two PRPs has been proved [DHT17] as described. Chen *et al.* [CLM19] studied the sum of Even-Mansour ciphers and proved its tight security of $2n/3$-bit.

2 Specification

Orthros is a 128-bit pseudorandom function (PRF) with a 128-bit key, the overview of which is illustrated in Fig 1. On the whole, Orthros consists of two SPN-based 128-bit keyed permutations called Branch1 and Branch2, each composed of an S-layer, P-layer, the round-key addition and the constant addition. The S-layer is the parallel application of a 4-bit S-box and the P-layer is a linear transform (bit or nibble permutation, followed by a matrix multiplication). Moreover, two key scheduling functions called KSF1 and KSF2 based on two different bit permutations are exploited in Branch1 and Branch2, respectively.

In Orthros, a 128-bit plaintext M[8] is first copied to two 128-bit internal states X^1 and X^2. Then X^1 and X^2 are respectively given to Branch1 and Branch2.

[7] `https://github.com/subhadeep-banik/orthros`

[8] For convenience, we may call an input (an output) of Orthros a plaintext (a ciphertext), although it is not a block cipher.

The 128-bit ciphertext C is an XOR of the outputs of Branch1 and Branch2. More details will be given in the following.

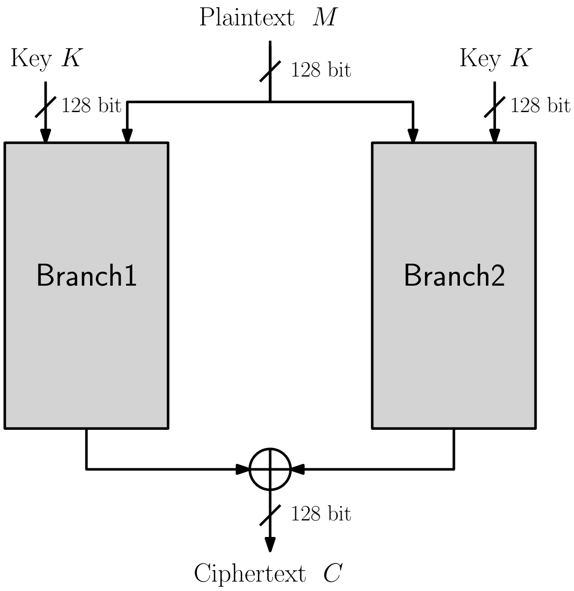

Fig. 1: Overview of Orthros.

2.1 Key Scheduling Function

Orthros adopts two bit-permutation-based key scheduling functions called KSF1 and KSF2, which are used to generate RK_r^1 and RK_r^2 $(0 \leq r \leq 12)$ from the same 128-bit key K for Branch1 and Branch2, respectively. The whitening keys are RK_0^1 and RK_0^2, which will be first XORed with X^1 and X^2, respectively. RK_r^1 and RK_r^2 $(1 \leq r \leq 12)$ are the round keys used in the r-th round of Branch1 and Branch2, respectively. The algorithms of KSF1 and KSF2 are shown in Fig 2. The bit-permutation P_{bk1} and P_{bk2} used in KSF1 and KSF2 are shown in Table 3.

In Fig 2, when K and RK_r^j are expressed in bit level, we have $RK_r^j = (rk_{r,0}^j, rk_{r,1}^j \cdots rk_{r,127}^j)$ and $K = (k_0, k_1 \cdots k_{127})$, where $rk_{r,i}^j, k_i \in F_2$ $(0 \leq i \leq 127, j \in \{1,2\})$. In addition, $rk_{r,0}^j$ and k_0 are the most significant bit of RK_r^j and K, respectively.

2.2 Round Function of Branch1 and Branch2

In this section, we present the details of Branch1 and Branch2, each of which is a 128-bit keyed permutation consisting of 12 rounds. The round keys (and

```
Algorithm KSF1($K$)

($k_0 \parallel k_1 \parallel \cdots \parallel k_{127}$) ← $K$
for $r = 0$ to 12 do
    ($rk^1_{r,0} \parallel rk^1_{r,1} \parallel \cdots \parallel rk^1_{r,127}$) ← $RK^1_r$
    if $r = 0$ then
        for $i = 0$ to 127 do
            $rk^1_{0,P_{bk1}(i)} \leftarrow k_i$
        end for
    else
        $rk^1_{r,P_{bk1}(i)} \leftarrow rk^1_{r-1,i}$
    end if
end for
for $r = 0$ to 12 do
    $RK^1_r \leftarrow (rk^1_{r,0} \parallel rk^1_{r,1} \parallel \cdots \parallel rk^1_{r,127})$
end for
return $(RK^1_0, RK^1_1, \cdots RK^1_{12})$
```

```
Algorithm KSF2($K$)

($k_0 \parallel k_1 \parallel \cdots \parallel k_{127}$) ← $K$
for $r = 0$ to 12 do
    ($rk^2_{r,0} \parallel rk^2_{r,1} \parallel \cdots \parallel rk^2_{r,127}$) ← $RK^2_r$
    if $r = 0$ then
        for $i = 0$ to 127 do
            $rk^2_{0,P_{bk2}(i)} \leftarrow k_i$
        end for
    else
        $rk^2_{r,P_{bk2}(i)} \leftarrow rk^2_{r-1,i}$
    end if
end for
for $r = 0$ to 12 do
    $RK^2_r \leftarrow (rk^2_{r,0} \parallel rk^2_{r,1} \parallel \cdots \parallel rk^2_{r,127})$
end for
return $(RK^2_0, RK^2_1, \cdots RK^2_{12})$
```

Fig. 2: Algorithms of KSF1 and KSF2.

whitening keys) (RK^1_r, RK^2_r) are first generated by KSF1 and KSF2. After adding the whitening keys, the 128-bit input will be processed via Branch1 and Branch2 as follows.

For the first 4 rounds of Branch1 and Branch2, the round function R is described as

$$R = \texttt{AddConstant} \circ \texttt{AddRoundKey} \circ \texttt{matrixMul} \circ \texttt{bit-permutation} \circ \texttt{S-box},$$

where `AddConstant` and `AddRoundKey` represent the constant addition operation and the round key addition operation, respectively.

For the following 7 rounds, the round function R' is described as

$$R' = \texttt{AddConstant} \circ \texttt{AddRoundKey} \circ \texttt{matrixMul} \circ \texttt{nibble-permutation} \circ \texttt{S-box}.$$

The sequence of operations in the last round is `AddConstant` ∘ `AddRoundKey` ∘ `S-box`. As described, the 128-bit outputs of Branch1 and Branch2 are XORed to generate the 128-bit ciphertext. Each component in the round function of Branch1 and Branch2 is described as follows.

S-box (`S-box`). A 4-bit S-box will be applied to each nibbles in parallel for Branch1 and Branch2. The specification of the 4-bit S-box is displayed in Table 1.

Table 1: S-box in Branch1 and Branch2.

x	0	1	2	3	4	5	6	7	8	9	a	b	c	d	e	f
$S(x)$	1	0	2	4	3	8	6	d	9	a	b	e	f	c	7	5

Permutation (`bit-permutation`, `nibble-permutation`). For the first 4 rounds of Branch1 and Branch2, P_{br1} and P_{br2} will be used respectively. From the

5th round to the 11th round, the nibble permutations P_{n1} and P_{n2} will be adopted in each branch respectively. The details of the permutation P_{brN} and P_{nN}, where $N \in \{1,2\}$, are shown in Table 4 and Table 5, respectively.

Matrix Multiplication (`matrixMul`). Let $\boldsymbol{M_b}$ be 4×4 matrix over nibbles defined as

$$\boldsymbol{M_b} = \begin{pmatrix} 0\,1\,1\,1 \\ 1\,0\,1\,1 \\ 1\,1\,0\,1 \\ 1\,1\,1\,0 \end{pmatrix}.$$

Four nibbles (a_0, a_1, a_2, a_3) will be updated as follows:

$$(a_0, a_1, a_2, a_3)^T \leftarrow \boldsymbol{M_b} \cdot (a_0, a_1, a_2, a_3)^T,$$

where $(a_0, a_1, a_2, a_3)^T$ denotes a transposition. Specifically,

$$\begin{aligned} a_0 &= a_1 \oplus a_2 \oplus a_3, \\ a_1 &= a_0 \oplus a_2 \oplus a_3, \\ a_2 &= a_0 \oplus a_1 \oplus a_3, \\ a_3 &= a_0 \oplus a_1 \oplus a_2. \end{aligned}$$

AddRoundKey (`AddRoundKey`). In the r-th round, the internal states in Branch1 and Branch2 will be xored with the corresponding round key RK_r^1 and RK_r^2, respectively.

AddConstant (`AddConstant`). The internal state will be xored with the corresponding round constant in each branch. The specification of the round constants is displayed in Table 2, where RC_r^1 and RC_r^2 represent the round constant used in the r-th round of Branch1 and Branch2, respectively.

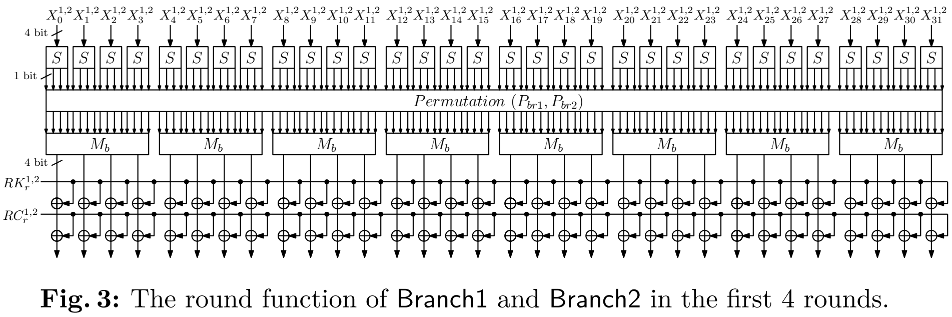
$X_0^{1,2}$ $X_1^{1,2}$ $X_2^{1,2}$ $X_3^{1,2}$ … $X_{31}^{1,2}$
4 bit
S
1 bit
Permutation (P_{br1}, P_{br2})
M_b
4 bit
$RK_r^{1,2}$
$RC_r^{1,2}$

Fig. 3: The round function of Branch1 and Branch2 in the first 4 rounds.

Table 2: Specification of the round constants RC_r^1 and RC_r^2.

Branch1	
Round Number r	RC_r^1
1	0xa0ac9329ac4bc991c2313219c193ca81
2	0x4420cb8b49cc9ba882c104ba4a22c918
3	0x3c0b2031431044cc31401a4129a108b8
4	0x33cc10a4043289941183323849c22304
5	0xaa82c1118b929aca0409424088ba2814
6	0x2081380c9c290882aacb223114a44aa4
7	0x981c0cb22144084bab32c99a2309423a
8	0xb24119bc33c18b2938900c848a2b242b
9	0x3491a301a430822a1933241099c9b039
10	0x301248a0939b922c380330318aac40ba
11	0x440a904904b141492a048b8a9b21b3c4
12	0x92c81b00089982982a44102332909c20

Branch2	
Round Number r	RC_r^2
1	0xa34a8ca0a88b04a1982b9381b2bacac8
2	0xca98490c308b9c0c99308bc988288c2a
3	0x403a2311bccb13a4ab39a8c42ba93924
4	0x48913c9c0c1808ca4894c19b399b1220
5	0x32b3218430109ca4a31ca91239b8c838
6	0x10bcc304a1b813b829c90b8bb1498bb3
7	0xa91c233a40c233b34a028990002b4093
8	0x8a2931ab0413bc2bb89a13abbc4b048b
9	0x9b1b8bc390a342204809124a9a180a32
10	0xa4ac29b88283c913cb4492c491aa100c
11	0xcab089094810cb043201a20c0acc09b1
12	0x4bba3b8984cb028c3839089a4cccccc1

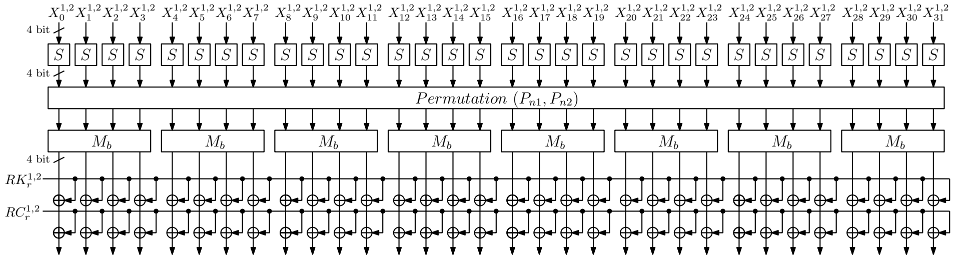
$X_0^{1,2}$ $X_1^{1,2}$ $X_2^{1,2}$ $X_3^{1,2}$ … $X_{31}^{1,2}$
4 bit
S
4 bit
$Permutation\ (P_{n1}, P_{n2})$
M_b
4 bit
$RK_r^{1,2}$
$RC_r^{1,2}$

Fig. 4: The round function of Branch1 and Branch2 in the last 8 rounds. The nibble permutation and the matrix multiplication in the last round will be omitted.

Round Constants. In a similar manner to PRINCE, the round constants are derived from the fraction part of $\pi = 3.1415926....$ Specifically, if the fraction part of $\pi = 3.1415926...$ is expressed in binary string, it will be `0001010000010101 1001....` By shifting left the binary string by 3 bits, we obtain a binary string `1010 0000 1010 1100 1`..., which corresponds to a nibble string `0xa`, `0x0`, `0xa`, `0xc`, and so on.

Illustration of Round Function. The illustration of the round function in the first 4 rounds of Branch1 and Branch2 is shown in Fig 3. The illustration of the round function in the last 8 rounds is shown in Fig 4.

Pseudocode. The algorithms of Branch1 and Branch2 are shown in Fig 5. In the pseudocode, when the 128-bit internal state is expressed in bits, we have $X = (x_0, x_1, \cdots x_{127})$ and x_0 is the most significant bit of X. When the 128-bit internal state is expressed in nibbles, we have $X = (X_0, X_1, \ldots, X_{31})$ and X_0 is the most significant nibble of X. For the constant addition, the 128-bit round constant RC_r^j is expressed in nibbles as $RC_r^j = (RC_{r,0}^j, RC_{r,1}^j, \cdots, RC_{r,31}^j)$, for $1 \leq r \leq 12$ and $1 \leq j \leq 2$, where j denotes the index of Branch. Similarly for the round-key addition, the 128-bit round key RK_r^j is expressed in nibbles as $RK_r^j = (RK_{r,0}^j, RK_{r,1}^j, \ldots, RK_{r,31}^j)$, for $1 \leq r \leq 12$ and $1 \leq j \leq 2$.

Processing. The 128-bit ciphertext C is generated by XORing the output of Branch1 and Branch2. The processing algorithm of Orthros is shown in Fig 6. We provide test vectors of Orthros in Appendix E.

Claimed Security. Orthros claims single-key security, and does not claim any security in related-key and known/chosen-key settings.

3 Design Rationale

3.1 General Construction

As described in introduction, the overall structure of Orthros is a sum of two keyed permutations. This structure and its variant has been extensively studied in the literature [Luc00, BI99, Pat08, DHT17, CLM19, Iwa06]. In particular, if two keyed permutations of Orthros (Branch1 and Branch2) were independent PRPs, we could claim n-bit provable security – more specifically the PRF advantage of $(q/2^n)^{1.5} + 2\epsilon(q, t + O(q))$ for $n = 128$ and q adaptive queries and time complexity t, where $\epsilon(q, t)$ denotes the PRP advantages of Branch1 and Branch2 with q queries and t time [DHT17]. However, this means that either Branch1 or Branch2 could be already usable as a low-latency PRP, implying that they should have a sufficient amount of security margins against known cryptanalysis. Since each Branch never gives its outputs in clear, we expect that a pair of weak permutations can suffice to have a desired, n-bit secure PRF. Generally this approach is described as "prove-then-prune" [HKR15]. This means that the provable security reduction does not hold anymore, and an implication of the security bound is more or less

```
**Algorithm** Branch$N(K, X)$

$(RK_0^N \,\|\, RK_1^N \,\|\, \ldots \,\|\, RK_{12}^N) \leftarrow \mathsf{KSF}N(K)$
$X \leftarrow X \oplus RK_0^N$
$(X_0 \,\|\, X_1 \,\|\, \ldots \,\|\, X_{31}) \leftarrow X$
for $r = 1$ to $11$ do
    $(RC_{r,0}^N \,\|\, RC_{r,1}^N \,\|\, \ldots \,\|\, RC_{r,31}^N) \leftarrow RC_r^N$
    $(RK_{r,0}^N \,\|\, RK_{r,1}^N \,\|\, \ldots \,\|\, RK_{r,31}^N) \leftarrow RK_r^N$
    for $i = 0$ to $31$ do
        $X_i \leftarrow S(X_i)$
    end for
    if $r < 5$ then
        for $i = 0$ to $31$ do
            $(x_{4i} \,\|\, x_{4i+1} \,\|\, x_{4i+2} \,\|\, x_{4i+3}) \leftarrow X_i$
        end for
        $(x'_0, x'_1, \ldots, x'_{127}) \leftarrow (x_0, x_1, \ldots, x_{127})$
        for $i = 0$ to $127$ do
            $x_{P_{brN}(i)} \leftarrow x'_i$
        end for
        for $i = 0$ to $31$ do
            $X_i \leftarrow (x_{4i} \,\|\, x_{4i+1} \,\|\, x_{4i+2} \,\|\, x_{4i+3})$
        end for
    else
        $(X'_0, X'_1, \ldots, X'_{31}) \leftarrow (X_0, X_1, \ldots, X_{31})$
        for $i = 0$ to $31$ do
            $X_{P_{nN}(i)} \leftarrow X'_i$
        end for
    end if
    for $i = 0$ to $7$ do
        $(X_{4i}, X_{4i+1}, X_{4i+2}, X_{4i+3})^T \leftarrow \boldsymbol{M_b} \cdot (X_{4i}, X_{4i+1}, X_{4i+2}, X_{4i+3})^T$
    end for
    for $i = 0$ to $31$ do
        $X_i \leftarrow X_i \oplus RK_{r,i}^N \oplus RC_{r,i}^N$
    end for
end for
for $i = 0$ to $31$ do
    $X_i \leftarrow S(X_i)$
end for
$(RC_{12,0}^N \,\|\, RC_{12,1}^N \,\|\, \ldots \,\|\, RC_{12,31}^N) \leftarrow RC_{12}^N$
$(RK_{12,0}^N \,\|\, RK_{12,1}^N \,\|\, \ldots \,\|\, RK_{12,31}^N) \leftarrow RK_{12}^N$
for $i = 0$ to $31$ do
    $X_i \leftarrow X_i \oplus RK_{12,i}^N \oplus RC_{12,i}^N$
end for
$Y \leftarrow (X_0 \,\|\, X_1 \,\|\, \ldots \,\|\, X_{31})$
return $Y$
```

Fig. 5: Algorithms of Branch1 and Branch2, where $N \in \{1, 2\}$.

```
**Algorithm** Orthros$(K, M)$

$X^1 \leftarrow M$, $X^2 \leftarrow M$
$Y^1 \leftarrow$ Branch1$(K, X^1)$, $Y^2 \leftarrow$ Branch2$(K, X^2)$
$C \leftarrow Y^1 \oplus Y^2$
return $C$
```

Fig. 6: Processing algorithm of Orthros.

Table 3: Bit permutation P_{bkN} for key scheduling $\mathsf{KSF}N$, where $N \in \{1, 2\}$.

x	0	1	2	3	4	5	6	7	8	9	10	11	12	13	14	15
$P_{bk1}(x)$	0	53	87	73	22	95	99	48	61	36	108	1	24	67	119	93
$P_{bk2}(x)$	76	30	53	35	31	46	2	79	11	125	110	87	39	91	14	101
x	16	17	18	19	20	21	22	23	24	25	26	27	28	29	30	31
$P_{bk1}(x)$	54	103	69	112	16	111	94	122	31	66	33	83	47	3	65	62
$P_{bk2}(x)$	97	118	36	48	29	80	57	115	49	18	74	85	61	82	105	126
x	32	33	34	35	36	37	38	39	40	41	42	43	44	45	46	47
$P_{bk1}(x)$	123	9	101	19	5	58	89	37	38	51	28	106	82	76	121	4
$P_{bk2}(x)$	70	12	47	111	51	17	66	1	60	96	116	71	81	114	104	15
x	48	49	50	51	52	53	54	55	56	57	58	59	60	61	62	63
$P_{bk1}(x)$	70	7	42	92	104	80	45	75	114	17	2	97	46	107	63	18
$P_{bk2}(x)$	42	124	100	4	113	44	75	89	23	0	84	107	32	26	88	8
x	64	65	66	67	68	69	70	71	72	73	74	75	76	77	78	79
$P_{bk1}(x)$	109	15	127	43	13	59	29	125	77	11	50	30	12	90	118	64
$P_{bk2}(x)$	69	121	38	94	37	86	54	21	62	123	41	10	16	95	117	65
x	80	81	82	83	84	85	86	87	88	89	90	91	92	93	94	95
$P_{bk1}(x)$	20	35	57	10	124	56	68	91	116	21	84	98	52	81	126	34
$P_{bk2}(x)$	45	50	72	20	109	58	7	67	108	28	3	55	92	103	24	5
x	96	97	98	99	100	101	102	103	104	105	106	107	108	109	110	111
$P_{bk1}(x)$	105	27	120	74	6	85	40	72	113	41	23	49	79	55	102	8
$P_{bk2}(x)$	77	9	27	102	122	6	106	22	99	34	90	56	43	83	120	64
x	112	113	114	115	116	117	118	119	120	121	122	123	124	125	126	127
$P_{bk1}(x)$	117	39	88	26	25	110	14	32	115	100	86	71	78	44	96	60
$P_{bk2}(x)$	78	59	119	93	40	98	52	68	112	33	63	25	19	73	127	13

Table 4: Bit permutation P_{brN} for round function $\mathsf{Branch}N$, where $N \in \{1, 2\}$.

x	0	1	2	3	4	5	6	7	8	9	10	11	12	13	14	15
$P_{br1}(x)$	6	46	62	126	70	52	28	14	36	125	72	83	106	95	4	35
$P_{br2}(x)$	20	122	74	62	119	35	15	66	9	85	32	117	21	83	127	106
x	16	17	18	19	20	21	22	23	24	25	26	27	28	29	30	31
$P_{br1}(x)$	25	41	10	76	87	74	120	42	88	21	11	67	64	38	112	50
$P_{br2}(x)$	11	98	115	59	71	90	56	26	2	44	103	121	114	107	68	16
x	32	33	34	35	36	37	38	39	40	41	42	43	44	45	46	47
$P_{br1}(x)$	85	109	24	65	99	0	49	37	8	66	114	47	127	100	56	40
$P_{br2}(x)$	84	1	102	33	80	52	76	36	27	94	37	55	82	12	112	64
x	48	49	50	51	52	53	54	55	56	57	58	59	60	61	62	63
$P_{br1}(x)$	13	117	78	86	92	58	124	101	55	89	97	9	18	116	59	15
$P_{br2}(x)$	105	14	91	17	108	124	6	93	29	86	123	79	72	53	19	99
x	64	65	66	67	68	69	70	71	72	73	74	75	76	77	78	79
$P_{br1}(x)$	20	45	75	2	77	27	1	60	115	107	26	69	119	3	84	51
$P_{br2}(x)$	50	18	81	73	67	88	4	61	111	49	24	45	57	78	100	22
x	80	81	82	83	84	85	86	87	88	89	90	91	92	93	94	95
$P_{br1}(x)$	123	110	31	82	113	53	81	102	63	118	93	12	30	94	108	32
$P_{br2}(x)$	110	47	116	54	60	70	97	39	3	41	48	96	23	42	113	87
x	96	97	98	99	100	101	102	103	104	105	106	107	108	109	110	111
$P_{br1}(x)$	5	111	29	43	91	19	79	33	73	44	98	48	22	61	68	105
$P_{br2}(x)$	126	13	31	40	51	25	65	125	8	101	118	28	38	89	5	104
x	112	113	114	115	116	117	118	119	120	121	122	123	124	125	126	127
$P_{br1}(x)$	34	71	54	104	17	57	80	103	96	121	23	39	122	90	7	16
$P_{br2}(x)$	109	120	69	43	7	77	58	34	10	63	30	95	75	46	0	92

Table 5: Nibble permutation P_{nN} for round function $\mathsf{Branch}N$, where $N \in \{1, 2\}$.

x	0	1	2	3	4	5	6	7	8	9	10	11	12	13	14	15
$P_{n1}(x)$	10	27	5	1	30	23	16	13	21	31	6	14	0	25	11	18
$P_{n2}(x)$	26	13	7	11	29	0	17	21	23	5	18	25	12	10	28	2
x	16	17	18	19	20	21	22	23	24	25	26	27	28	29	30	31
$P_{n1}(x)$	15	28	19	24	7	8	22	3	4	29	9	2	26	20	12	17
$P_{n2}(x)$	14	19	24	22	1	8	4	31	15	6	27	9	16	30	20	3

fuzzy and depends on the scheme. In our analysis we did not find a full-round attack against Branch1 and Branch2 as a PRP, however they have rather slim margins as a standalone block cipher. Therefore, we bolster our security claim with an extensive security analysis on the whole construction.

We note that realizing Branch1 and Branch2 as Even-Mansour ciphers [EM93] can reduce the circuit size thanks to the absence of key schedule. However, it can provide $2n/3$-bit PRF security at best, as proved by Chen *et al.* [CLM19]. Instead, we adopt bit permutation-based key scheduling functions for its hardware friendliness.

In order to investigate the initial security of the sum of permutations from the perspective of cryptanalysis, we compare in Appendix A the differential and linear behaviour for two toy ciphers adopting single branch and double branches, respectively. However, it should be emphasized that the security of Orthros never relies on our experiments on the toy ciphers but rather a comprehensive study of Orthros, as will be detailed in Section 4.

3.2 Linear Layer

As underlying matrices in the linear layer, we adopt 4×4 almost MDS binary matrix used in Midori [BBI$^+$15], whose delay is much smaller than MDS matrices. However, as discussed in [BBI$^+$15], its diffusion speed is slower and the lower bounds of the number of active S-boxes in each round is smaller than those of ciphers employing MDS matrices due to its lower branch number. To improve the diffusion speed and to increase active S-boxes in each round, we utilize bit and nibble permutations in a hybrid manner. We will see that this enables to guarantee security with a relatively small number of rounds.

Midori-128 [BBI$^+$15] also adopted a bit and a nibble permutations, however, our design is more efficient in term of the diffusion speed and the number of active S-boxes while keeping the same hardware cost in an unrolled implementation. Specifically, we adopt two different linear layers that consists of a bit permutation and a nibble permutation, *i.e.*, a bit permutation is used for some rounds and a nibble permutation for the rest, while Midori-128 [BBI$^+$15] uses a single linear layer including both of a bit permutation and a nibble permutation. Importantly, this change of linear layers does not require any additional hardware cost in an unrolled implementation, as observed by [BCG$^+$12].

Bit Permutation vs Nibble Permutation. To see the advantage of our hybrid use of bit and nibble permutations over the consistent use of a bit or a nibble permutation, we compare the diffusion effect and the lower bound of the number of active S-boxes of two different 128-bit block SPN structures, which we call SPN-B and SPN-N. Here, SPN-B (SPN-N) consistently uses a bit (nibble) permutation. Both use the same 4-bit S-box and the matrix as those used in a branch of Orthros. In addition, we used the full-diffusion property of S-box when evaluating the diffusion effect.

Diffusion. To evaluate the minimum number of rounds that achieves the full diffusion for each SPN-B and SPN-N, we look into the propagation of one active input bit and count the upper bounds of the number of active bits through each operation. Here, we only need to consider the number of active bits after `S-box` and `matrixMul` as the remaining operations do not affect its value. The upper bounds of the number of active bits after each operation over some rounds are shown in Table 6.

Table 6: The upper bound of the number of active bits after each operation.

Round	**Operation**	**Structures**	
		SPN-B	SPN-N
-	Input	1	1
1	`S-box`	4	4
	`matrixMul`	12	12
2	`S-box`	48	12
	`matrixMul`	120	36
3	`S-box`	**128**	36
	`matrixMul`	128	100
4	`S-box`	128	100
	`matrixMul`	128	**128**

According to Table 6, SPN-B and SPN-N require at least 2.5 rounds (2 rounds plus `S-box`) and 4 rounds, respectively, *i.e.*, the *optimal* numbers of rounds for the full diffusion of SPN-B and SPN-N are estimated as 2.5 and 4 rounds, respectively. We conclude that there is a clear gap between bit permutations and nibble permutations in terms of the diffusion. Note that a class of bit permutations covers all nibble permutations. Thus, to achieve the 2.5-round full diffusion, we need to find a class of bit permutations that are not included in a class of nibble permutations.

Active S-box. Mixed Integer Linear Programming (MILP) is used to obtain the lower bound of the number of active S-boxes in each round. Unfortunately, it is computationally infeasible to estimate the lower bound of the number of active S-boxes of SPN-B, except for a very small number of rounds, due to the large search space of 128-bit bitwise differential and linear trails. This problem about the use of bit permutation was also pointed out by the designers of QARMA-128 [Ava17]. As a consequence, QARMA-128 does not claim a lower bound of active S-boxes. Indeed, it was infeasible to compute a lower bound of the number of active S-boxes for more than 5 rounds for SPN-B, even with a computer equipped with 48 cores and 256 GB RAM. Therefore, SPN-B can only guarantee a very small number of active S-boxes for a moderately large number of rounds (say 10), since we have to combine the bounds obtained for a small number of rounds, which generally yields a loose bound. For example, the lower bound for 8 rounds is obtained by the sum of the bounds for 4 rounds. In our experiment, the best lower bound for 4 rounds is 16, therefore the obtained bound for 8 rounds is only 32.

On the other hand, for SPN-N, it is feasible to obtain a tight lower bound of the number of active S-boxes up to 8 rounds, using the aforementioned 48-core computer. The evaluation of one candidate requires about 2 days by the same computer. As a result, we found a class of nibble permutations that attain 60 active S-boxes over 8 rounds. We will explain the details in the following section.

Conclusion. Based on the above discussions, we conclude that a structure employing a single permutation cannot achieve a fast full diffusion and a guaranteed large number of active S-boxes simultaneously. Hence, we decided to use a bit permutation for the first few rounds, and use a nibble permutation for the rest of the rounds. Consequently, Orthros reaches the full diffusion after first 2.5 rounds and guarantees more than 64 active S-boxes over 10 rounds.

Finding Optimal Bit Permutations for Diffusion. We take a two-step approach to find a class of bit permutations that achieves 2.5-round full diffusion for SPN-B, which turns out to be optimal. Let S denote the 128-bit internal state S of SPN-B. It is also viewed as a 4×8 two-dimensional nibble array:

$$S = \begin{bmatrix} S_0 & S_4 & S_8 & S_{12} & S_{16} & S_{20} & S_{24} & S_{28} \\ S_1 & S_5 & S_9 & S_{13} & S_{17} & S_{21} & S_{25} & S_{29} \\ S_2 & S_6 & S_{10} & S_{14} & S_{18} & S_{22} & S_{26} & S_{30} \\ S_3 & S_7 & S_{11} & S_{15} & S_{19} & S_{23} & S_{27} & S_{31} \end{bmatrix},$$

where S_i $(0 \leq i \leq 31)$ is a 4-bit value defined as

$$S_i \ = \ [s_{4i}, s_{4i+1}, s_{4i+2}, s_{4i+3}]^T.$$

Note that S can also be viewed as a 16×8 two-dimensional binary array by seeing each column of S as a 16-bit sequence. Hereafter, *bit-cell* means a binary cell in the 16×8 array and *nibble-cell* means a nibble cell in the 4×8 array, that is, S_i.

We first try to reduce the search space of target 128-bit permutations as it is computationally infeasible to test all possible $2^{716.16}(= 128!)$ candidates. Specifically, we focus on a class satisfying Condition 1 to efficiently find the class of bit permutations having the 2.5 rounds full diffusion property.

Condition 1 *For any nibble-cell S_i $(0 \leq i \leq 31)$, the corresponding 4 bits, $s_{4i}, s_{4i+1}, s_{4i+2}, s_{4i+3}$, are mapped to the bit-cells in different columns after applying the bit permutation.*

A detailed description of Condition 1 can be seen in Appendix B.1.

Condition 1 can be justified as follows. If a bit permutation satisfies Condition 1, for the 4 output bits of each S-box, they will be mapped to 4 different groups of inputs to the binary matrix. Observe that in the MatrixMul operation, the binary matrix M_b is independently applied to 8 different groups of inputs, each of which consists of 4 consecutive nibbles. This is expected to be a key feature for the fast diffusion since 1 input active bit is expanded to 4 active bits via the S-box, and the 4 active bits are subsequently expanded to 12 active bits after the bit permutation and MatrixMul operations. This matches the upper bound of the number of active bits after one-round permutation, as shown in Table 6.

In the class of the bit permutations satisfying Condition 1, we obtain the following sufficient condition for the 2.5-round full diffusion. It should be emphasized that for each active bit in the nibble-cell S_i $(0 \leq i \leq 31)$, after applying the S-box and the bit permutation satisfying Condition 1, there will exist 4 different groups of inputs to the binary matrix, each of which will contain exactly one active nibble. Therefore, after matrixMul there will be 12 active nibbles. We add the following condition on these 12 active nibbles.

Condition 2 *After applying the bit permutation, in each column of the* 4×8 *array, there exist at least 2 nibble-cells containing the bits coming from those in the active 12 nibbles.*

The proof that Condition 2 is sufficient for the 2.5 round full diffusion in the class of the bit permutations satisfying Condition 1 is described in Appendix B.2.

Bit permutations of Table 4 used in Branch1 and Branch2 satisfy both Condition 1 and 2, respectively, i.e. attain 2.5-round full diffusion.

Finding Good Nibble Permutation for Active S-boxes. As in the case of bit permutations, we take the following two-step approach to find nibble permutations that can activate as many S-boxes as possible over a certain number of rounds, which is expected to outperform that used in Midori-128. To explain our approach, we use the same 4×8 array to express the 128-bit state as above.

In the first step, we reduce the search space by focusing on the class of nibble permutations satisfying Condition 3 since it is computationally infeasible to estimate the lower bound of the number of active S-boxes for all possible $2^{117.66}(= 32!)$ permutations. Condition 3 is chosen to achieve fast diffusion for differences and linear masks.

Condition 3 *For each column* $(S_{4i}, S_{4i+1}, S_{4i+2}, S_{4i+3})$ *in the* 4×8 *array, after applying the nibble permutation, they will be mapped to four nibble-cells in different columns.*

In the second step, we first randomly choose 7,000 nibble permutations satisfying Condition 3. Then, we compute the lower bound of the number of active S-boxes after 5, 6, 7 and 8 rounds for these nibble permutations. To efficiently find good permutations among these nibble permutations, we first find a class of nibble permutations that have the best lower bound after 5 rounds.

Then, we focus on this class and evaluate the lower bound of the number of active S-boxes after 6 rounds, which will be repeated until the 8th round.

As a result, we find three nibble permutations that can achieve 60 active S-boxes over 8 rounds. Table 7 shows the comparison of the lower bound of the number of active S-boxes for Midori-128 and our structure. Compared with Midori-128, our nibble permutations guarantee a much larger number of active S-boxes after 6 rounds, about a factor of 1.5.

Table 7: Comparison of lower bounds of the number of active S-boxes.

Target	4	5	6	7	8
Midori-128 [BBI+15]	16	20	30	35	38
Our nibble permutation	16	25	36	51	60

Hybrid Use of Bit and Nibble Permutations. Consequently, we obtain a set of bit and nibble permutations. For Orthros, we pick a bit and nibble permutations from the set, and use the bit permutation for the first 4 rounds, in order to achieve a fast full diffusion. Specifically, it achieves full diffusion in 2.5 rounds, while Midori-128 requires 3 rounds. For the rest of 8 rounds we used the nibble permutation to guarantee a large number of active S-boxes. Indeed, 10 rounds of Orthros starting from the 3rd round, *i.e.*, the 3rd to the 12th round, achieve 64 active S-boxes. We note that Midori-128 needs 13 rounds to obtain 64 active S-boxes, thus the gain is 3 rounds.

3.3 S-box

We search a small-delay and lightweight 4-bit S-box which fulfills the following requirements: (1) the maximal probability of a differential is 2^{-2}, (2) the maximal absolute bias of a linear approximation is 2^{-2} and (3) full diffusion, *i.e.*, any input bit difference diffuses to all output bits. We use a metric called *depth* [BBI+15] to estimate the path delay of S-boxes.

Definition 1 (depth): *The depth is defined as the sum of the sequential path delays of basic operations, namely* `AND`*,* `OR`*,* `NAND`*,* `NOR` *and* `NOT`*.*

Following the assumption of [BBI+15], our search assumes that depths of `XOR`, `AND`/`OR`, `NAND`/`NOR`, and `NOT` are weighted as 2, 1.5, 1 and 0.5, respectively, and the required gates of `NOT`, `NAND`/`NOR`, `AND`/`OR` and `XOR`/`XNOR` are estimated as 0.5, 1, 1.5 and 2 Gate Equivalents (GEs), respectively. We search over the set of all 4-bit S-boxes, whose size is $2^{44.3}$, sort them in order of small depth, and check whether they satisfy our security requirements.

We remark that our construction does not require the involution property of S-box unlike Midori's Sb_1. It allows us to expand the number of possible candidates from $2^{25.5}$ (the number of all involution 4-bit S-boxes) to $2^{44.3}$. As a result, we found an S-box (see Table 1) whose depth and gate size are the lowest and the smallest in our search. Specifically, the depth is 3.5 and the area is 20 GE under the aforementioned assumption of [BBI+15]. The S-box can be expressed as follows[9], where inputs and outputs are defined as $\{x_0, x_1, x_2, x_3\}$ and $\{y_0, y_1, y_2, y_3\}$, and x_3 and y_3 are the most significant bits.

$$\begin{aligned}
y_0 &= \Big((x_0 \texttt{ NOR } x_3) \texttt{ AND } x_1\Big) \texttt{ NOR } \Big((x_1 \texttt{ NAND } x_2) \texttt{ AND } x_0\Big)\\
y_1 &= \Big((x_1 \texttt{ NOR } x_2) \texttt{ OR } x_0\Big) \texttt{ NAND } \Big((x_0 \texttt{ NAND } x_3) \texttt{ OR } x_2\Big)\\
y_2 &= \Big((x_1 \texttt{ OR } x_3) \texttt{ NAND } x_2\Big) \texttt{ NAND } (x_0 \texttt{ NAND } x_1)\\
y_3 &= \Big((x_1 \texttt{ NAND } x_2) \texttt{ NAND } x_3\Big) \texttt{ NAND } \Big((x_0 \texttt{ NAND } x_2) \texttt{ OR } x_3\Big)
\end{aligned}$$

Compared to the S-box of Midori-128, the depth and area can be reduced to 3.5 and 10.7 GE from 4 and 12 GE, respectively, when synthesized with the standard cell library of the STM 90nm CMOS logic process (as shown in Table 8) with area optimization. The table also shows detailed comparisons with S-boxes of the QARMA and PRINCE family when the circuit is optimized with respect to area as well as delay. The S-box of Orthros performs well when optimized across both metrics. Note that σ_0 does not have the full diffusion property.

Table 8: Comparison of S-boxes.

	Orthros	Midori [BBI+15]	QARMA [Ava17]				PRINCE [BCG+12]	
	S	Sb_1	σ_0	σ_1	σ_2	σ_2^{-1}	S	S^{-1}
Area Optimized								
Area [GE]	**10.7**	12.0	11.0	12.2	15.7	15.5	12.2	15.5
Delay [ps]	**285.7**	367.2	380.6	412.3	328.3	531.3	341.9	390.7
Delay Optimized								
Area [GE]	**40.4**	32.2	43.2	36.4	40.2	65.4	51.1	41.2
Delay [ps]	**37.2**	71.1	39.2	89.3	58.6	53.3	52.7	80.6
Full diffusion	**Yes**	Yes	No	Yes	Yes	Yes	Yes	Yes
Involution	No	Yes	Yes	Yes	No	No	No	No

3.4 Key Scheduling Function

To minimize the hardware cost, key scheduling functions of Orthros are realized by only bit permutations, whose hardware overhead, such as area and delay, is essentially free. We use a class of bit permutations that satisfy both Condition 1 and 2 in the key scheduling functions of Branch1 and Branch2 as shown in Table 3, although it cannot guarantee the full diffusion property as there is no S-box and

[9] We fixed the typos in the expressions in [BIL+21]

Matrix in the key scheduling functions. One reason to introduce two different key scheduling functions for each branch is to increase the hardness of the key-recovery attack, as will be discussed in the next section.

4 Security Evaluation

4.1 Differential/Linear Attack

To evaluate the resistance against differential attacks and linear attacks, one way is to obtain the lower bound of the number of differentially and linearly active S-boxes in each round, which can be efficiently computed with a MILP-based method [MWGP11]. In the following, we will present lower bounds of the number of differentially and linearly active S-boxes for Branch1, Branch2 and the whole Orthros. Since the maximal differential and linear probability of the S-box is 2^{-2}, it is sufficient to guarantee the security against differential attacks and linear attacks if there are 64 active S-boxes, as it gives $2^{-2\times 64} = 2^{-128}$ as an estimate of a differential probability. In our evaluation, we only consider the single-key setting.

As discussed in Section 3.2, we observed that it is computationally infeasible to obtain a lower bound for more than 5 rounds starting from the first round of Branch1, Branch2 and Orthros, even with a computer equipped with 48 cores and 256 GB RAM. The search space of 128-bit bitwise differential and linear trails for the first 4 rounds is huge. On the other hand, for the last 8 rounds of Branch1 and Branch2 starting from the 5th round, where the nibble permutation is adopted, we can obtain tight lower bounds of the number of active S-boxes for the nibble-wise differential and linear trails. In addition, we can obtain tight lower bounds of the number of active S-boxes of 5 rounds of Orthros starting from the 5th round, *i.e.*, 5 to 9 rounds.

In our evaluation, each of Branch1, Branch2 and Orthros is first divided into two parts, *i.e.*, the first 4 rounds and the remaining 8 rounds. We compute a lower bound of the number of active S-boxes for each part. The lower bound of Orthros is obtained by the sum of those of Branch1 and Branch2.

The corresponding results are displayed in Table 9. Table 9 shows that there are at least 68 active S-boxes in 5 rounds of Orthros starting from the 5th round, *i.e.*, 5 to 9 rounds. In addition, the last 10 rounds of Branch1 and Branch2 including 2 bit-permutation rounds and 8 nibble-permutation rounds, *i.e.*, 3 to 12 rounds, have at least $64(= 4 + 60)$ active S-boxes. Although we do not claim any security for Branch1 and Branch2 as a full-fledged block cipher, each has a sufficient number of active S-boxes in the full 12 rounds.

It should be emphasized that the lower bounds of Orthros in Table 9 are not tight *i.e.*, actually the full rounds of Orthros includes more active S-boxes. This is because the number of active S-boxes of Orthros after 10 rounds is computed as the sum of those of Branch1 and Branch2. Besides, those of first 4 rounds and the last 8 rounds are independently obtained. Thus, we expect that the full-round Orthros can resist against the differential attack and the linear attack.

Table 9: The lower bounds of the number of active S-boxes in the single-key setting.

Construction	**bit/nibble**	**Rounds**											
		1	**2**	**3**	**4**	**5**	**6**	**7**	**8**	**9**	**10**	**11**	**12**
Orthros (the first 4 rounds)	bit	2	8	12	16	-	-	-	-	-	-	-	-
Orthros (from the 5th round)	nibble	-	-	-	-	2	8	20	40	**68**	72	101	120
Branch1 (the first 4 rounds)	bit	1	4	6	8	-	-	-	-	-	-	-	-
Branch2 (the first 4 rounds)	bit	1	4	5	8	-	-	-	-	-	-	-	-
Branch1 (from the 5th round)	nibble	-	-	-	-	1	4	7	16	25	36	50	60
Branch2 (from the 5th round)	nibble	-	-	-	-	1	4	7	16	25	36	51	60

4.2 Impossible Differential Attack

The impossible differential attack can be estimated by the required number of rounds for the full diffusions. In the forward direction, both Branch1 and Branch2 require 2.5 rounds for the full diffusion, while it is 5 rounds in the backward direction. Consequently, we expect that there is no any probability-one impossible differential characteristic over 8 rounds of Branch1 and Branch2, respectively. Since Orthros take a sum of the outputs of Branch1 and Branch2, we believe that the number of rounds of an impossible differential characteristic for Orthros is much lower than that of Branch1 and Branch2.

To obtain actual impossible differential characteristics, we utilize the MILP-aided automatic searching tool proposed by Sasaki and Todo [ST17]. Taking DDT (differential distribution table) of the S-box into consideration, we searched bit-wise impossible differential characteristics of Orthros that have one active bit for both of a plaintext and a ciphertext. The details of modeling S-boxes is in Appendix C.2

As a result, we found 3/5/5-round impossible differential characteristics of Orthros, Branch1 and Branch2, respectively, as shown in Appendix C.3. Thus, we expect that the full-round Orthros is secure against impossible differential attacks.

4.3 Integral Attack

We present integral distinguishers on round-reduced Orthros. Since the division property [Tod15, TM16] was proposed, it has become an efficient tool to evaluate the resistance against integral attacks. Moreover, with the development of the MILP model for the bit-based division property [XZBL16], the attacker now only needs to focus on modeling the propagation of the division property.

The round function of Orthros consists of a nonlinear layer (`S-box`), a bit/nibble permutation layer, another linear layer (`matrixMul`) and the constant/key addition. To model the propagation of the division property through each component, we only need to consider the S-box and the binary matrix used in `matrixMul`. The bit/nibble permutation only has an influence on the coordinates of the variables used in the MILP model. The modelling of the S-box and binary matrix can be referred to Appendix C.4.

Based on our model, the longest integral distinguisher can reach up to at most 7 rounds with 127 active bits in the input. For example, when the most significant bit of the plaintext is constant and the remaining 127 bits take all possible 2^{127} values, for 7-round Orthros, all output bits are balanced.

Remark. Although there are several 7-round integral distinguishers, it is difficult to mount a key-recovery attack on 8 rounds of Orthros. This is different from usual key-recovery attacks on block ciphers, where the attacker is able to add several rounds after the integral distinguisher and guess partial key bits to decrypt the ciphertext. It is quite costly to guess the key bits and reverse the ciphertext for Orthros since the final output is the sum of the outputs of two branches, *i.e.*, the attacker further needs to guess the output of the other branch.

4.4 Invariant Subspace Attack

Beierle *et al.* [BCLR17] showed that an invariant subspace attack can be mounted on a block cipher if one finds a non-trivial invariant for the substitution layer whose linear space is invariant under the linear layer matrix L that it uses and contains all the differences between the round keys. For block ciphers without a dedicated key schedule function, say when the i-th round key $rk_i = k \oplus rc_i$ is simply the xor of the master key and the i-th round constant, the difference of all round keys is the difference of the round constants. If D denotes the set of all round constant differences, the authors of [BCLR17] computed $W_L(D)$, which denotes the smallest L-invariant subspace containing D. If the dimension of $W_L(D)$, $\dim(W_L(D))$, satisfies $\dim(W_L(D)) \geq n-1$, where n is the block size of the cipher in bits, then the authors showed that there is no non-trivial invariant of the substitution layer, provided that the S-box is well designed and does not have any linear component.

If this condition is not satisfied, one must further investigate the properties of the substitution layer. The authors then showed that, for every subspace Z of the 0-linear space of the invariant of the substitution layer S, the invariant, g, takes the same value on each coset of Z in $\mathbb{F}_2^n$ and also on each element of the set $S(Z)$. To show that g is trivial, the authors computed the S-box layer at some points in Z and hoped that all cosets would be hit when evaluating S at a few points in Z. If g takes the same value on all the corresponding cosets, we would conclude that g must be a constant function and thus trivial. This can be done if we take $Z = W_L(D)$ and if $\dim(W_L(D))$ is close to n, since one would only need to hit $2^{n-\dim(W_L(D))}$ cosets.

Since our construction uses a key schedule function for both branches, we can not directly construct the set D as the difference of round constants. From this fact, we use four different linear layers (two different in each branch) in our construction. However for any randomly chosen value of the secret key k one can construct the sets D_1, D_2, D_3, D_4, one each for the difference of the round keys used in each of the four linear layers L_1, L_2, L_3, L_4, and then try to compute $\dim(W_{L_i}(D_i))$ for each i. We found that the linear matrices composed by a bit permutation and a matrix multiplication (used in the first to 4th rounds of each branch, call them L_1 (left), L_3 (right)) have extremely high multiplicative orders – around 2^{48} to 2^{60} – and thus it is not directly possible to find $W_L(D)$ for these matrices. Thus we limited ourselves to find $W_L(D)' = \sum_{c \in D} < L^i(c),\ i \leq 10000 >$ for L_1, L_2 and L_3 (where $< \cdot >$ denotes the subspace generated by the constituent vectors). We did an experiment with 1000 randomly chosen keys, and computed $W_{L_i}(D_i), W_{L_i}(D_i)'$. The dimension of these spaces is almost always more than 127 for L_1, L_3 and always more than 123 for L_2, L_4. Whenever the dimension of these spaces was less than 127, we tried to run Algorithm 1 of [BCLR17] to see if all cosets are hit when trying to evaluate the S-layer. For all choices of the random key, we find that all the cosets are always hit, and thus we conclude that it is highly unlikely that an invariant subspace attack can be mounted on our construction.

4.5 Meet-in-the-Middle Attack

To mount a meet-in-the middle attack, the adversary has to compute the inverse of the cipher, *i.e.*, computing intermediate states (matching states) from the corresponding ciphertexts by guessing the involved round keys. As discussed above, the adversary needs to guess one of two 128-bit outputs of branches to go through the final XOR operation in the backward computation. As it requires at least 2^{128} iterations, the attack is not efficient than the brute force attack.

Another possibility is to use the splice-and-cut technique [SA09]. With this technique, the adversary guesses the intermediate values as the start point from which the adversary starts the computation toward both directions. However, once she guesses a 128-bit intermediate of one branch, she has to correctly guess the corresponding 128-bit intermediate of the other branch. Therefore, we believe that Orthros is secure against meet-in-the middle attacks.

4.6 Yoyo and Mixture-Differential Attacks

The yoyo attack was first introduced by Biham [BBD+99]. Recently, it has been applied to the cryptanalysis of AES by Rønjom *et al.* [RBH17], where generic attacks on up to 3 rounds of SPNs have been discussed. Since 2-round AES can be viewed as 1-round SPN with the concept of super S-box, distinguishing attack on up to 6 rounds of AES are derived by [RBH17]. However, there is one major step in the yoyo attack, that is, the attacker needs to make a decryption query. For the design of Orthros, since the final output is the xor sum of the outputs of Branch1 and Branch2, it is infeasible to make a decryption query. In addition, due to the fast diffusion of the bit permutation and the fact that each branch adopts a different bit permutation, it is quite difficult to construct an efficient super S-box for Orthros in the first four rounds. Based on these reasons, we believe that Orthros is resistant against such an attack.

In Asiacrypt 2019, a different view of the yoyo attack on AES, called exchange attack, was proposed by Bardeh and Rønjom [BR19]. It does not require decryption queries and can reach up to 6 rounds of AES. However, due to the similarity in the underlying idea between the yoyo attack and exchange attack, we believe that the resistance against the yoyo attack implies the resistance against exchange attack.

The mixture differential introduced by Grassi [Gra18] is an efficient tool to analyze a reduced-round AES, as its contribution to the recent progress of key-recovery attacks on 5-round AES [BDK$^+$18, DKRS20]. An important factor which makes the mixture differential efficient is that AES adopts a word-wise permutation. Due to the effect of the bit permutation in the first four rounds, we are not able to find a useful mixture differential for Orthros.

4.7 Difficulty of Key-Recovery Attacks

As we repeated several times, the unique feature of Orthros (as a cryptographic primitive) is that it takes the sum of two branch outputs. To mount a key-recovery attack with a statistical distinguisher for block ciphers, such as a differential/linear/integral distinguisher, it is common to append a few rounds after a certain number of rounds for which a distinguisher exists, and guess partial key bits by partially decrypting the ciphertext and verifying whether the distinguishing property holds. However, such a common strategy is quite hard for Orthros since the attacker even needs to guess the outputs of each branch in order to reverse the ciphertext. In addition, it is required to construct two distinguishers for two different branches with the same plaintext set simultaneously if the attacker wants to append a few rounds after the distinguishable rounds. Even if it is possible to construct a distinguisher for one block cipher with an advanced cryptanalysis method as discussed above, it would be challenging to construct two different distinguishers for two different block ciphers for the same plaintext set simultaneously. In such a situation, we think generally the most promising direction is to find integral distinguishers. This will be discussed later.

Another attacking strategy is to prepend some rounds before the distinguishable rounds. However, this implies that there exists a distinguisher for each branch simultaneously. When extending two distinguishers backwards to the plaintext, the attacker can derive which key bits should be guessed in order to compute the desired value of the intermediate internal state of both branches. Since each branch adopts a different linear layer in its round function, and the key schedules of two branches also differ, a lot of to-be-guessed key bits will be involved. Moreover, the whitening keys in two branches are different as well, which further increases the complexity to prepend some rounds before a distinguisher. For better understanding, we present a framework to recover the secret key by extending an integral distinguisher backwards.

A Framework for Recovering the Secret Key. This framework was once applied to a preliminary version of Orthros. Therefore, we omit the details of the design and explain a high-level idea. First, we denote the states after the S-box layer in the first round of Branch1 and Branch2 by $XL^{0.5}$ and $XR^{0.5}$, respectively. Suppose there is a set of bit positions denoted by $PSet \subseteq \{i \mid 0 \leq i \leq 127\}$ and the size of $PSet$ is $PSize$. In addition, let us denote the final output after r rounds of (an old version of) $\mathsf{Orthros}$ by C^r, which is the sum of the outputs of (old versions of) $\mathsf{Branch1}$ and $\mathsf{Branch2}$. Suppose there is an integral distinguisher such that

$$\sum C^r = \sum_{XL^{0.5} \in PS} \mathsf{Branch1}(XL^{0.5}) \oplus \sum_{XR^{0.5} \in PS'} \mathsf{Branch2}(XR^{0.5}) = 0,$$

where $PS, PS' \in \{e \in \mathbb{F}_2^{128} \mid e[i] \in \{0,1\}, i \in PSet\}$, *i.e.*, the set of values whose bits located at the positions belonging to $PSet$ take all the possible 2^{PSize} values and the remaining $(128 - PSize)$ bits take constant values.

To mount a key recovery attack, the attacker first derives from $PSet$ the active bits in the plaintext. Specifically, if $i \in PSet$, the $(4 \times i/4)$-th, $(4 \times i/4 + 1)$-th, $(4 \times i/4 + 2)$-th and $(4 \times i/4 + 3)$-th bits of the plaintext are all active. Let $ASize$ be the size of the active bits in the plaintext. The attacker then prepares a plaintext set whose active bits take all possible values and make encryption queries with the r-round $\mathsf{Orthros}$. It is easily detected that the sum of the ciphertext is zero. Record the corresponding 2^{ASize} pairs of plaintext and ciphertext in a table.

Suppose the whitening keys used by $\mathsf{Branch1}$ and $\mathsf{Branch2}$ are the same. In this case, the attacker guesses 2^{ASize} different values of the whitening key which is xored with the active bits in the input. For each guess, the attacker can partially know the corresponding $XL^{0.5}$ and $XR^{0.5}$ and can divide the plaintext set into $2^{ASize-PSize}$ different subsets according to the value of the nonactive bits of $XL^{0.5}$ and $XR^{0.5}$ via the constructed integral distinguisher. For each subset, compute the sum of the corresponding ciphertexts. For the correct key, the sum will be zero for all subsets. However, for a wrong key, the sum is zero for a subset with a probability 2^{-128}. Therefore, the attacker can recover the key bits by checking the sum of the ciphertexts for the plaintexts in each subset.

Consider the case when different whitening keys are used for $\mathsf{Branch1}$ and $\mathsf{Branch2}$. In this case, when the attacker guesses the key bits in the left branch to obtain the corresponding $2^{ASize-PSize}$ subsets of the plaintexts, the sum of the ciphetexts for the plaintexts in each subset is not clear even the guess is correct. This is because the set of $XR^{0.5}$ behaves randomly for each subset of plaintext obtained according to the guess of the whitening key used in $\mathsf{Branch1}$.

Obviously, it can be interpreted that this framework for $\mathsf{Orthros}$ is to convert a r-round distinguisher into a r-round key-recovery attack. Therefore, a long distinguisher should be prevented in our design.

5 Hardware Evaluation

Since our target construction is a low-latency PRF, the most useful hardware evaluation of the design is a fully unrolled circuit that optimizes the signal delay from the input to output ports. Such a circuit would be able to evaluate the PRF in one clock cycle itself, and naturally the clock frequency can be increased till the clock period is just above the total critical path of the circuit, affording a maximum throughput of $\frac{blocksize}{critical\ path}$ bits per second. To perform a fair evaluation we compare our construction with two other low-latency primitives that provide at least 128-bit block and 128-bit security. The first is Midori-128 and the second is QARMA$_9$-128-σ_0 (in [Ava17], QARMA with 9 forward and backward rounds was recommended for applications targeting 192 bit security). QARMA$_9$-128-σ_0 is a particular instantiation of QARMA with 9 forward and backward rounds and a low-delay S-box σ_0. For an added comparison, we also include the 64-bit block cipher PRINCE in our results. On the other hand we also benchmark some permutation based constructions that can be used as a PRF. For example the Kangaroo12-XOF [BDP$^+$18] which is based on the 12-round Keccak-f[1600] permutation can be used as a PRF: one could absorb the key and plaintext in the permutation state and extract 128 bits from the resulting XOF. Let us call this construction Kangaroo12-PRF[1600]. Since any design based on a 1600-bit state would naturally be hardware-intensive we also consider a lightweight version of the above construction Kangaroo12-PRF[400] based on the 12-round Keccak-f[400] permutation. We can also use the Subterranean-Deck function [DMMR20] to extract a 128 bit MAC from a 128 bit key and message. We also benchmark this design which we call Subterranean-PRF. It is even more lightweight as it has only a 257-bit state.

We found that across all libraries, Orthros even outperforms PRINCE (see Tables 10, 18, 19, 17) when it comes to the absolute signal delay between the input/output ports. We remark that PRINCE is a 64-bit block cipher.

For a fair evaluation we adhered to the following design flow for all the ciphers:

1. The RTL source codes for the circuit of the ciphers were first written in the Verilog HDL, and a functional simulation was done using the Modelsim software to ensure correctness.
2. The RTL codes were synthesized by the *Synopsys Design Vision* circuit compiler, with the compiler command set to `compile_ultra`. No other optimizations are done at this stage. For this process we used the standard cell libraries of the following CMOS logic processes: **a)** STM 90nm, **b)** TSMC 90nm, **c)** Nangate 45nm and **d)** Nangate 15nm.
3. A timing simulation was done on the synthesized netlist to confirm the correctness of the design, by comparing the output of the timing simulation with known test vectors.
4. The switching activity of each gate of the circuit was collected while running post-synthesis simulation. The average power was obtained using *Synopsys Power Compiler*, using the back annotated switching activity.
5. Step 2 outputs the critical path of the circuit. We repeat steps 2-4 (for each of the libraries) but this time by asking the circuit compiler to constrain the total signal delay between the input/output ports to some value less than the critical path computed in step 2.
6. We repeat the above processes, with progressively lower values of total signal delay, till such time as the circuit compiler is unable to construct a circuit with given delay. We stop the flow at this point. All results have been tabulated in Tables 10, 17, 18, 19 (for space constraints Tables 17, 18, 19 showing results for Nangate 15nm, TSMC 90nm and Nangate 45 nm processes are shifted to Appendix D).

Cipher	Area		Power	Energy	Latency	Max TP
	(μm^2)	(GE)	(mW)	(pJ)	(ns)	(Gbps)
Orthros	98150.7	22307	6.647	664.69	10.60	11.246
	99258.2	22559	6.025	602.50	9.00	13.245
	102286.4	23247	6.214	621.40	8.00	14.901
	108582.3	24678	7.220	722.02	7.00	17.030
	123160.6	27991	9.612	961.24	6.00	19.868
	133931.3	30430	10.751	1075.07	5.00	23.842
	148432.8	33735	12.614	1261.35	4.00	29.802
	177991.2	40453	16.591	1659.12	3.00	39.736
	298855.6	67922	27.628	2762.76	2.40	49.671
Midori-128	85435.0	19417	10.205	1020.49	18.54	6.430
	86470.0	19652	9.671	967.14	16.00	7.451
	89648.7	20375	9.748	974.81	14.00	8.515
	96225.5	21869	11.275	1127.54	12.00	9.934
	107393.6	24408	15.687	1568.7	10.00	11.921
	122584.4	27860	17.887	1788.72	8.00	14.901
	144109.4	32752	24.011	2401.09	5.99	19.868
	277950.7	63171	46.464	4646.39	4.10	29.075
QARMA$_9$-128-σ_0	104118.3	23663	10.044	1004.38	19.41	6.142
	104686.9	23792	9.810	981.04	17.00	7.012
	106848.1	24284	9.911	991.05	15.00	7.947
	112157.2	25490	11.571	1157.09	13.00	9.170
	128032.8	29098	16.816	1681.62	11.00	10.837
	147874.2	33608	20.438	2043.83	9.00	13.245
	182268.6	41425	27.714	2771.37	6.96	17.128
	234453.9	53285	41.508	4150.79	4.99	23.890
	319634.3	72644	58.119	5811.87	4.38	27.217
PRINCE	27897.7	6340	1.867	186.73	11.35	10.503
	28773.6	6539	1.791	179.13	9.00	13.245
	31905.0	7251	2.057	205.67	7.00	17.030
	38941.7	8850	3.274	327.44	5.00	23.842
	63795.8	14499	6.023	602.25	3.00	39.736
	87285.5	19838	8.151	815.12	2.56	46.566
Kangaroo12-PRF[1600] *	498909.7	113389	59.533	5953.25	17.52	6.804
	552581.2	125587	58.170	5817.01	12.00	9.934
	590922.6	134301	57.350	5735.03	8.00	14.901
	1184290.6	269157	140.664	14066.38	3.99	29.877
Kangaroo12-PRF[400] *	133662.4	30378	16.674	1667.36	18.47	6.454
	144600.0	32864	14.388	1438.84	12.00	9.934
	167258.9	38013	18.260	1825.96	8.00	28.725
	339374.6	77131	39.311	3931.14	4.15	14.901
Subterranean-PRF *	130206.1	29592	9.976	997.59	17.45	6.831
	139879.2	31791	8.467	846.6	12.00	9.934
	177843.0	40419	18.475	1847.46	8.00	14.901
	375592.1	85362	40.271	4027.13	3.63	32.840

Table 10: Results for the STM 90nm library. Power measured at 10 MHz. *The core implementation of the underlying permutations in these constructions were taken from [BDH$^+$, DMMR]

Why area increases with decrease in latency: A cell library typically has several drive strengths of cells that implement a given logic function. These drive strengths correspond to the capacitive load that a cell can drive without excessive delay and with acceptable signal characteristics. Thus when we force the circuit compiler to construct a circuit with lower delay, it starts introducing higher drive strength gates, that typically occupy more area while offering the same functionality. For example, in the TSMC 90nm library 2-input xor gates of drive strength 1, 2 ,4 occupy around 2.5, 3, 5 GE respectively. Thus it is natural for the area of a circuit to progressively increase as we constrain the circuit compiler to construct circuits of increasingly lower delay as shown in Tables 10, 17, 18, 19.

For a better illustrative purposes, we provide *Area vs Delay* (see Fig. 7). The plots tell us that not only does Orthros perform around 40% better across all standard cell libraries when it comes to the absolute delay value, it also outperforms QARMA$_9$-128-σ_0 and Midori-128 when it comes to achieving **a)** lower area figures and power consumption given a particular delay budget and **b)** lower or competitive delay given a particular area/power budget.

6 Conclusions

We have presented a new low-latency PRF of 128-bit block, dubbed Orthros. The design is essentially a sum of keyed permutations, which has been studied in the context of provable security. We found this design is suitable to a low-latency cryptographic primitive, which is intuitive, however, to our knowledge never seriously considered before. We made it real by thoroughly revising the current state-of-the-art low-latency, lightweight building blocks, together with an extensive security analysis and comprehensive hardware benchmarks.

For further directions, it would be interesting to extend our design, say having more branches (with even simpler round functions or fewer rounds), to even reduce latency. Software performance and related-key/side-channel security would also be interesting topics.

Acknowledgments

The authors would like to thank the anonymous reviewers for their valuable comments and suggestions. The authors also thank Zihao Wei for pointing out some typos in Section 3.3. Subhadeep Banik is supported by the Swiss National Science Foundation (SNSF) through the Ambizione Grant `PZ00P2_179921`. Takanori Isobe is supported by JST, PRESTO Grant Number JPMJPR2031, Grant-in-Aid for Scientific Research (B)(KAKENHI 19H02141) for Japan Society for the Promotion of Science, and Support Center for Advanced Telecommunications Technology Research (SCAT). Kosei Sakamoto is supported by Grant-in-Aid for JSPS Fellows (KAKENHI 20J23526) for Japan Society for the Promotion of Science.

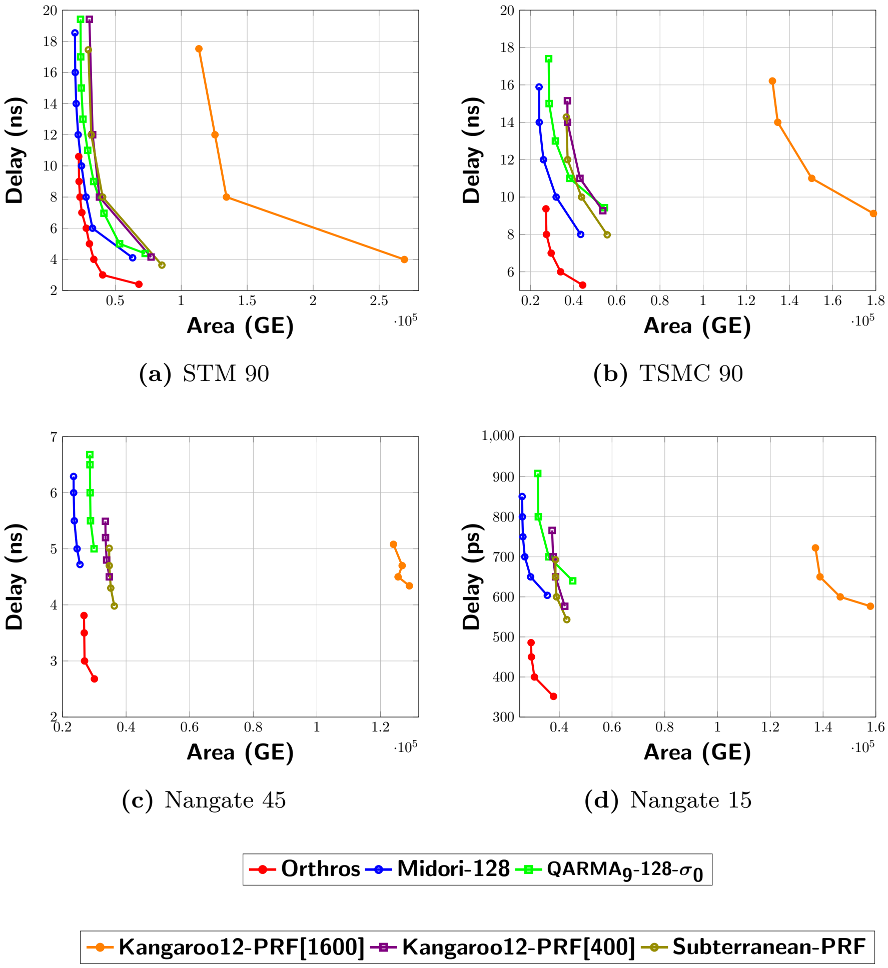

(a) STM 90

(b) TSMC 90

(c) Nangate 45

(d) Nangate 15

Fig. 7: Delay vs Area comparisons.

References

[Ava17] Roberto Avanzi. The QARMA block cipher family. *IACR Trans. Symm. Cryptol.*, 2017(1):4–44, 2017. `doi:10.13154/tosc.v2017.i1.4-44`.

[BBD+99] Eli Biham, Alex Biryukov, Orr Dunkelman, Eran Richardson, and Adi Shamir. Initial observations on Skipjack: Cryptanalysis of Skipjack-3XOR (invited talk). In Stafford E. Tavares and Henk Meijer, editors, *SAC 1998*, volume 1556 of *LNCS*, pages 362–376. Springer, Heidelberg, August 1999. `doi:10.1007/3-540-48892-8_27`.

[BBI+15] Subhadeep Banik, Andrey Bogdanov, Takanori Isobe, Kyoji Shibutani, Harunaga Hiwatari, Toru Akishita, and Francesco Regazzoni. Midori:

A block cipher for low energy. In Tetsu Iwata and Jung Hee Cheon, editors, *ASIACRYPT 2015, Part II*, volume 9453 of *LNCS*, pages 411–436. Springer, Heidelberg, November / December 2015. doi:10.1007/978-3-662-48800-3_17.

[BCG$^+$12] Julia Borghoff, Anne Canteaut, Tim Güneysu, Elif Bilge Kavun, Miroslav Knežević, Lars R. Knudsen, Gregor Leander, Ventzislav Nikov, Christof Paar, Christian Rechberger, Peter Rombouts, Søren S. Thomsen, and Tolga Yalçin. PRINCE - A low-latency block cipher for pervasive computing applications - extended abstract. In Xiaoyun Wang and Kazue Sako, editors, *ASIACRYPT 2012*, volume 7658 of *LNCS*, pages 208–225. Springer, Heidelberg, December 2012. doi:10.1007/978-3-642-34961-4_14.

[BCLR17] Christof Beierle, Anne Canteaut, Gregor Leander, and Yann Rotella. Proving resistance against invariant attacks: How to choose the round constants. In *Advances in Cryptology - CRYPTO 2017 - 37th Annual International Cryptology Conference, Santa Barbara, CA, USA, August 20-24, 2017, Proceedings, Part II*, pages 647–678, 2017. doi:10.1007/978-3-319-63715-0_22.

[BDH$^+$] Guido Bertoni, Joan Daemen, Seth Hoffert, Michaël Peeters, Gilles Van Assche, and Ronny Van Keer. Team keccak: Hardware resources. https://keccak.team/hardware.html.

[BDK$^+$18] Achiya Bar-On, Orr Dunkelman, Nathan Keller, Eyal Ronen, and Adi Shamir. Improved key recovery attacks on reduced-round AES with practical data and memory complexities. In Hovav Shacham and Alexandra Boldyreva, editors, *CRYPTO 2018, Part II*, volume 10992 of *LNCS*, pages 185–212. Springer, Heidelberg, August 2018. doi:10.1007/978-3-319-96881-0_7.

[BDP$^+$18] Guido Bertoni, Joan Daemen, Michaël Peeters, Gilles Van Assche, Ronny Van Keer, and Benoît Viguier. Kangarootwelve: Fast hashing based on keccak-p. In *Applied Cryptography and Network Security - 16th International Conference, ACNS 2018, Leuven, Belgium, July 2-4, 2018, Proceedings*, pages 400–418, 2018. doi:10.1007/978-3-319-93387-0_21.

[BGGS20] Zhenzhen Bao, Chun Guo, Jian Guo, and Ling Song. TNT: How to tweak a block cipher. In Vincent Rijmen and Yuval Ishai, editors, *EUROCRYPT 2020, Part II*, LNCS, pages 641–673. Springer, Heidelberg, May 2020. doi:10.1007/978-3-030-45724-2_22.

[BI99] M. Bellare and R. Impagliazzo. A tool for obtaining tighter security analyses of pseudorandom function based constructions, with applications to PRP to PRF conversion. Cryptology ePrint Archive, Report 1999/024, 1999. http://eprint.iacr.org/1999/024.

[BIL$^+$21] Subhadeep Banik, Takanori Isobe, Fukang Liu, Kazuhiko Minematsu, and Kosei Sakamoto. Orthros: A low-latency prf. *IACR Transactions on Symmetric Cryptology*, 2021(1):37–77, Mar. 2021. URL: https://tosc.iacr.org/index.php/ToSC/article/view/8833, doi:10.46586/tosc.v2021.i1.37-77.

[Bir07] Alex Biryukov. The design of a stream cipher LEX. In Eli Biham and Amr M. Youssef, editors, *SAC 2006*, volume 4356 of *LNCS*, pages 67–75. Springer, Heidelberg, August 2007. doi:10.1007/978-3-540-74462-7_6.

[BJK$^+$16] Christof Beierle, Jérémy Jean, Stefan Kölbl, Gregor Leander, Amir Moradi, Thomas Peyrin, Yu Sasaki, Pascal Sasdrich, and Siang Meng Sim. The SKINNY family of block ciphers and its low-latency variant MANTIS. In

Matthew Robshaw and Jonathan Katz, editors, *CRYPTO 2016, Part II*, volume 9815 of *LNCS*, pages 123–153. Springer, Heidelberg, August 2016. doi:10.1007/978-3-662-53008-5_5.

[BKL$^+$07] Andrey Bogdanov, Lars R. Knudsen, Gregor Leander, Christof Paar, Axel Poschmann, Matthew J. B. Robshaw, Yannick Seurin, and C. Vikkelsoe. PRESENT: An ultra-lightweight block cipher. In Pascal Paillier and Ingrid Verbauwhede, editors, *CHES 2007*, volume 4727 of *LNCS*, pages 450–466. Springer, Heidelberg, September 2007. doi:10.1007/978-3-540-74735-2_31.

[BPP$^+$17] Subhadeep Banik, Sumit Kumar Pandey, Thomas Peyrin, Yu Sasaki, Siang Meng Sim, and Yosuke Todo. GIFT: A small present - towards reaching the limit of lightweight encryption. In Wieland Fischer and Naofumi Homma, editors, *CHES 2017*, volume 10529 of *LNCS*, pages 321–345. Springer, Heidelberg, September 2017. doi:10.1007/978-3-319-66787-4_16.

[BR19] Navid Ghaedi Bardeh and Sondre Rønjom. The exchange attack: How to distinguish six rounds of AES with $2^{88.2}$ chosen plaintexts. LNCS, pages 347–370. Springer, Heidelberg, December 2019. doi:10.1007/978-3-030-34618-8_12.

[BS91] Eli Biham and Adi Shamir. Differential cryptanalysis of DES-like cryptosystems. In Alfred J. Menezes and Scott A. Vanstone, editors, *CRYPTO'90*, volume 537 of *LNCS*, pages 2–21. Springer, Heidelberg, August 1991. doi:10.1007/3-540-38424-3_1.

[BSS$^+$13] Ray Beaulieu, Douglas Shors, Jason Smith, Stefan Treatman-Clark, Bryan Weeks, and Louis Wingers. The SIMON and SPECK families of lightweight block ciphers. Cryptology ePrint Archive, Report 2013/404, 2013. http://eprint.iacr.org/2013/404.

[CLM19] Yu Long Chen, Eran Lambooij, and Bart Mennink. How to build pseudorandom functions from public random permutations. In Alexandra Boldyreva and Daniele Micciancio, editors, *CRYPTO 2019, Part I*, volume 11692 of *LNCS*, pages 266–293. Springer, Heidelberg, August 2019. doi:10.1007/978-3-030-26948-7_10.

[DBP96] Hans Dobbertin, Antoon Bosselaers, and Bart Preneel. RIPEMD-160: A strengthened version of RIPEMD. In Dieter Gollmann, editor, *FSE'96*, volume 1039 of *LNCS*, pages 71–82. Springer, Heidelberg, February 1996. doi:10.1007/3-540-60865-6_44.

[DDK09] Christophe De Cannière, Orr Dunkelman, and Miroslav Knežević. KATAN and KTANTAN - a family of small and efficient hardware-oriented block ciphers. In Christophe Clavier and Kris Gaj, editors, *CHES 2009*, volume 5747 of *LNCS*, pages 272–288. Springer, Heidelberg, September 2009. doi:10.1007/978-3-642-04138-9_20.

[DHT17] Wei Dai, Viet Tung Hoang, and Stefano Tessaro. Information-theoretic indistinguishability via the chi-squared method. In Jonathan Katz and Hovav Shacham, editors, *CRYPTO 2017, Part III*, volume 10403 of *LNCS*, pages 497–523. Springer, Heidelberg, August 2017. doi:10.1007/978-3-319-63697-9_17.

[DIS$^+$18] Patrick Derbez, Tetsu Iwata, Ling Sun, Siwei Sun, Yosuke Todo, Haoyang Wang, and Meiqin Wang. Cryptanalysis of AES-PRF and its dual. *IACR Trans. Symm. Cryptol.*, 2018(2):161–191, 2018. doi:10.13154/tosc.v2018.i2.161-191.

[DKRS20] Orr Dunkelman, Nathan Keller, Eyal Ronen, and Adi Shamir. The retracing boomerang attack. In Vincent Rijmen and Yuval Ishai, editors, *EUROCRYPT 2020, Part I*, LNCS, pages 280–309. Springer, Heidelberg, May 2020. doi:10.1007/978-3-030-45721-1_11.

[DMMR] Joan Daemen, Pedro Maat Costa Massolino, Alireza Mehrdad, and Yann Rotella. The subterranean 2.0 cipher suite. https://cs.ru.nl/~joan/subterranean.html.

[DMMR20] Joan Daemen, Pedro Maat Costa Massolino, Alireza Mehrdad, and Yann Rotella. The subterranean 2.0 cipher suite. *IACR Trans. Symmetric Cryptol.*, 2020(S1):262–294, 2020. doi:10.13154/tosc.v2020.iS1.262-294.

[DR05a] Joan Daemen and Vincent Rijmen. A new MAC construction ALRED and a specific instance ALPHA-MAC. In Henri Gilbert and Helena Handschuh, editors, *FSE 2005*, volume 3557 of *LNCS*, pages 1–17. Springer, Heidelberg, February 2005. doi:10.1007/11502760_1.

[DR05b] Joan Daemen and Vincent Rijmen. The Pelican MAC function 2.0. Cryptology ePrint Archive, Report 2005/088, 2005. http://eprint.iacr.org/2005/088.

[Dwo05] Morris Dworkin. Recommendation for Block Cipher Modes of Operation: The CMAC Mode for Authentication. Standard, National Institute of Standards and Technology., 2005.

[Dwo10] Morris Dworkin. Recommendation for Block Cipher Modes of Operation: The XTS-AES Mode for Confidentiality on Storage Devices. Standard, National Institute of Standards and Technology., 2010.

[EM93] Shimon Even and Yishay Mansour. A construction of a cipher from a single pseudorandom permutation. In Hideki Imai, Ronald L. Rivest, and Tsutomu Matsumoto, editors, *ASIACRYPT'91*, volume 739 of *LNCS*, pages 210–224. Springer, Heidelberg, November 1993. doi:10.1007/3-540-57332-1_17.

[GKM+09] Praveen Gauravaram, Lars R. Knudsen, Krystian Matusiewicz, Florian Mendel, Christian Rechberger, Martin Schläffer, and Søren S. Thomsen. Grøstl - a SHA-3 candidate. In Helena Handschuh, Stefan Lucks, Bart Preneel, and Phillip Rogaway, editors, *Symmetric Cryptography, 11.01. - 16.01.2009*, volume 09031 of *Dagstuhl Seminar Proceedings*. Schloss Dagstuhl - Leibniz-Zentrum für Informatik, Germany, 2009. URL: http://drops.dagstuhl.de/opus/volltexte/2009/1955/.

[GM16] Shay Gueron and Nicky Mouha. Simpira v2: A family of efficient permutations using the AES round function. In Jung Hee Cheon and Tsuyoshi Takagi, editors, *ASIACRYPT 2016, Part I*, volume 10031 of *LNCS*, pages 95–125. Springer, Heidelberg, December 2016. doi:10.1007/978-3-662-53887-6_4.

[GPPR11] Jian Guo, Thomas Peyrin, Axel Poschmann, and Matthew J. B. Robshaw. The LED block cipher. In Bart Preneel and Tsuyoshi Takagi, editors, *CHES 2011*, volume 6917 of *LNCS*, pages 326–341. Springer, Heidelberg, September / October 2011. doi:10.1007/978-3-642-23951-9_22.

[Gra18] Lorenzo Grassi. Mixture differential cryptanalysis: a new approach to distinguishers and attacks on round-reduced AES. *IACR Trans. Symm. Cryptol.*, 2018(2):133–160, 2018. doi:10.13154/tosc.v2018.i2.133-160.

[Gue16] Shay Gueron. A memory encryption engine suitable for general purpose processors. Cryptology ePrint Archive, Report 2016/204, 2016. http://eprint.iacr.org/2016/204.

[HJ06] W. Eric Hall and Charanjit S. Jutla. Parallelizable authentication trees. In Bart Preneel and Stafford Tavares, editors, *SAC 2005*, volume 3897 of *LNCS*, pages 95–109. Springer, Heidelberg, August 2006. doi:10.1007/11693383_7.

[HKR15] Viet Tung Hoang, Ted Krovetz, and Phillip Rogaway. Robust authenticated-encryption AEZ and the problem that it solves. In Elisabeth Oswald and Marc Fischlin, editors, *EUROCRYPT 2015, Part I*, volume 9056 of *LNCS*, pages 15–44. Springer, Heidelberg, April 2015. doi:10.1007/978-3-662-46800-5_2.

[Iwa06] Tetsu Iwata. New blockcipher modes of operation with beyond the birthday bound security. In Matthew J. B. Robshaw, editor, *FSE 2006*, volume 4047 of *LNCS*, pages 310–327. Springer, Heidelberg, March 2006. doi:10.1007/11799313_20.

[KNR12] Miroslav Knežević, Ventzislav Nikov, and Peter Rombouts. Low-latency encryption - is "lightweight = light + wait"? In Emmanuel Prouff and Patrick Schaumont, editors, *CHES 2012*, volume 7428 of *LNCS*, pages 426–446. Springer, Heidelberg, September 2012. doi:10.1007/978-3-642-33027-8_25.

[LRW02] Moses Liskov, Ronald L. Rivest, and David Wagner. Tweakable block ciphers. In Moti Yung, editor, *CRYPTO 2002*, volume 2442 of *LNCS*, pages 31–46. Springer, Heidelberg, August 2002. doi:10.1007/3-540-45708-9_3.

[Luc00] Stefan Lucks. The sum of PRPs is a secure PRF. In Bart Preneel, editor, *EUROCRYPT 2000*, volume 1807 of *LNCS*, pages 470–484. Springer, Heidelberg, May 2000. doi:10.1007/3-540-45539-6_34.

[Mat94] Mitsuru Matsui. Linear cryptanalysis method for DES cipher. In Tor Helleseth, editor, *EUROCRYPT'93*, volume 765 of *LNCS*, pages 386–397. Springer, Heidelberg, May 1994. doi:10.1007/3-540-48285-7_33.

[MN17a] Bart Mennink and Samuel Neves. Encrypted Davies-Meyer and its dual: Towards optimal security using mirror theory. In Jonathan Katz and Hovav Shacham, editors, *CRYPTO 2017, Part III*, volume 10403 of *LNCS*, pages 556–583. Springer, Heidelberg, August 2017. doi:10.1007/978-3-319-63697-9_19.

[MN17b] Bart Mennink and Samuel Neves. Optimal PRFs from blockcipher designs. *IACR Trans. Symm. Cryptol.*, 2017(3):228–252, 2017. doi:10.13154/tosc.v2017.i3.228-252.

[MWGP11] Nicky Mouha, Qingju Wang, Dawu Gu, and Bart Preneel. Differential and linear cryptanalysis using mixed-integer linear programming. In Chuankun Wu, Moti Yung, and Dongdai Lin, editors, *Information Security and Cryptology - 7th International Conference, Inscrypt 2011, Beijing, China, November 30 - December 3, 2011. Revised Selected Papers*, volume 7537 of *Lecture Notes in Computer Science*, pages 57–76. Springer, 2011. doi:10.1007/978-3-642-34704-7_5.

[NIS07] Recommendation for Block Cipher Modes of Operation: Galois/Counter Mode (GCM) and GMAC. Technical report, 2007. National Institute of Standards and Technology.

[Pat08] Jacques Patarin. A proof of security in O(2n) for the xor of two random permutations. In Reihaneh Safavi-Naini, editor, *ICITS 08*, volume 5155 of *LNCS*, pages 232–248. Springer, Heidelberg, August 2008. doi:10.1007/978-3-540-85093-9_22.

[Qua] Qualcomm Technologies Inc. Pointer Authentication on ARMv8.3. https://www.qualcomm.com/media/documents/files/whitepaper-pointer-authentication-on-armv8-3.pdf.

[RBH17] Sondre Rønjom, Navid Ghaedi Bardeh, and Tor Helleseth. Yoyo tricks with AES. In Tsuyoshi Takagi and Thomas Peyrin, editors, *ASIACRYPT 2017, Part I*, volume 10624 of *LNCS*, pages 217–243. Springer, Heidelberg, December 2017. doi:10.1007/978-3-319-70694-8_8.

[SA09] Yu Sasaki and Kazumaro Aoki. Finding preimages in full MD5 faster than exhaustive search. In Antoine Joux, editor, *EUROCRYPT 2009*, volume 5479 of *LNCS*, pages 134–152. Springer, Heidelberg, April 2009. doi:10.1007/978-3-642-01001-9_8.

[SHW+14] Siwei Sun, Lei Hu, Peng Wang, Kexin Qiao, Xiaoshuang Ma, and Ling Song. Automatic security evaluation and (related-key) differential characteristic search: Application to SIMON, PRESENT, LBlock, DES(L) and other bit-oriented block ciphers. In Palash Sarkar and Tetsu Iwata, editors, *ASIACRYPT 2014, Part I*, volume 8873 of *LNCS*, pages 158–178. Springer, Heidelberg, December 2014. doi:10.1007/978-3-662-45611-8_9.

[SIH+11] Kyoji Shibutani, Takanori Isobe, Harunaga Hiwatari, Atsushi Mitsuda, Toru Akishita, and Taizo Shirai. Piccolo: An ultra-lightweight blockcipher. In Bart Preneel and Tsuyoshi Takagi, editors, *CHES 2011*, volume 6917 of *LNCS*, pages 342–357. Springer, Heidelberg, September / October 2011. doi:10.1007/978-3-642-23951-9_23.

[ST17] Yu Sasaki and Yosuke Todo. New impossible differential search tool from design and cryptanalysis aspects - revealing structural properties of several ciphers. In Jean-Sébastien Coron and Jesper Buus Nielsen, editors, *EUROCRYPT 2017, Part III*, volume 10212 of *LNCS*, pages 185–215. Springer, Heidelberg, April / May 2017. doi:10.1007/978-3-319-56617-7_7.

[TM16] Yosuke Todo and Masakatu Morii. Bit-based division property and application to simon family. In Thomas Peyrin, editor, *FSE 2016*, volume 9783 of *LNCS*, pages 357–377. Springer, Heidelberg, March 2016. doi:10.1007/978-3-662-52993-5_18.

[Tod15] Yosuke Todo. Structural evaluation by generalized integral property. In Elisabeth Oswald and Marc Fischlin, editors, *EUROCRYPT 2015, Part I*, volume 9056 of *LNCS*, pages 287–314. Springer, Heidelberg, April 2015. doi:10.1007/978-3-662-46800-5_12.

[XZBL16] Zejun Xiang, Wentao Zhang, Zhenzhen Bao, and Dongdai Lin. Applying MILP method to searching integral distinguishers based on division property for 6 lightweight block ciphers. In Jung Hee Cheon and Tsuyoshi Takagi, editors, *ASIACRYPT 2016, Part I*, volume 10031 of *LNCS*, pages 648–678. Springer, Heidelberg, December 2016. doi:10.1007/978-3-662-53887-6_24.

A Toy Ciphers

The unique feature of our design is the use of two parallel branches (effectively block ciphers). In order to investigate the generic security of this design, we introduce two toy ciphers using single branch and double branches as shown in Fig. 8. We focus on the maximal differential probability (MDP) [BS91] and linear

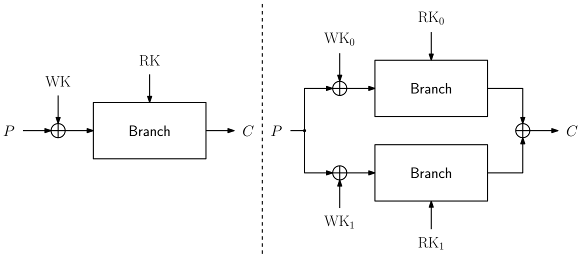

Fig. 8: (Left) The toy cipher using a single branch and (Right) that using double branches, where WK and RK are the whitening key and round key, respectively.

bias [Mat94] as they are two of the most fundamental security metrics. For the underlying branches, we consider both SPN and Feistel structures.

Experiments for a SPN-based toy cipher. First, we consider the case of SPN with 16-bit internal state and 16-bit round key. The basic design of this SPN-based toy cipher is similar to Midori. For our SPN-based toy cipher, the round function is composed of the following operations: S-box, Shuffle, Mix and AK. The state is organized as a 4×4 two-dimensional Boolean array A. The $(4j+i)$-th bit of the internal state is placed at $A[i][j]$ $(0 \leq i \leq 3, 0 \leq j \leq 3)$. For the S-box, each column $A[\cdot][j]$ $(0 \leq j \leq 3)$ is viewed as a 4-bit value $x = 8 \cdot A[3][j] + 4 \cdot A[2][j] + 2 \cdot A[1][j] + A[0][j]$ and the internal state is updated as $A[\cdot][j]$=S-box($A[\cdot][j]$). The S-box is the same with that used in Orthros. For the Shuffle operation, the state is reorganized as $A[i][j] = A[i'][j']$ $(0 \leq i \leq 3, 0 \leq j \leq 3)$, where $4j' + i' = \mathrm{SF}[4j+i]$ and the array SF is defined as

$$\mathrm{SF}[16] = [0, 10, 5, 15, 14, 4, 11, 1, 9, 3, 12, 6, 7, 13, 2, 8].$$

For the Mix operation, each column is updated by multiplying the binary matrix M_b, *i.e.*, $(A[0][j], A[1][j], A[2][j], A[3][j])^T = M_b \cdot (A[0][j], A[1][j], A[2][j], A[3][j])^T$ $(0 \leq j \leq 3)$. For the AK operation, a random 16-bit round key will be XORed with the 16-bit internal state. Since the construction of the underlying block cipher used in Orthros is somewhat similar to that of Midori, we adopt the same Shuffle and Mix operations as in Midori for the toy cipher in order to construct a 16-bit toy cipher.

To compute MDP over a certain number of rounds for each construction, we first generate a random value for the round keys. Then, the whole block cipher can be viewed as a large 16-bit S-box. By exhausting all possible $2^{16} \times (2^{16} - 1)/2$ input pairs, we count the number of occurrences for each possible output difference and obtain the maximum frequency of the output difference, which we denote by CNT_0. In this way, MDP is calculated as $\mathrm{CNT}_0/2^{16}$. With this method, we carried out 100 experiments and compute MDP for each experiments, and take the maximum for all experiments. The results are displayed in Table 11. Table 11 shows that the maximal value becomes stable after about 4 rounds in the construction using double branches. For the construction using a single branch, it becomes stable in about 5 rounds.

Table 11: The maximal differential probability of SPN-based toy ciphers.

Max Pro. Rounds	Single Branch	Double Branches
1	2^{-3}	2^{-1}
2	2^{-8}	2^{-6}
3	2^{-8}	$2^{-5.7}$
4	$2^{-11.3}$	$2^{-12.3}$
5	$2^{-12.5}$	$2^{-12.5}$
6	$2^{-12.5}$	$2^{-12.5}$
7	$2^{-12.5}$	$2^{-12.5}$
8	$2^{-12.5}$	$2^{-12.5}$

Experiments for a Feistel-based toy cipher. For the case of Feistel-based cipher, we consider 4-GFS (generalized Feistel structure with 4 sub-blocks), as shown in Fig. 9. The round function consists of two parallel 4-bit S-boxes with random round keys, where the S-box is the same with that used in Orthros. We carried out 100 experiments and compute the maximum of the MDP for all experiments, for both the constructions using a single branch and double branches. The corresponding results are displayed in Table 12. It shows that the maximal value becomes stable after about 7 rounds in the construction using double branches. For the construction using single branch, it becomes stable in about 10 rounds.

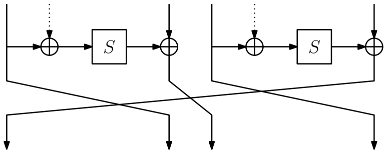

Fig. 9: 4-GFS. Dotted lines denote (random) round keys.

Experiments on linear masks. Similar experiments have also been performed to evaluate the maximal linear bias for the toy ciphers. Due to the high time complexity to accurately compute the maximal linear bias, we turn to calculating it in a probabilistic way. Specifically, we randomly choose some input and output masks and select the maximal linear bias from them. For the SPN-based toy cipher, it is found that the maximal linear bias ($2^{-6.4}$) becomes stable after 4 rounds if using a single branch, while it becomes stable in 3 rounds for double branches.

Table 12: The maximal differential probability for each GFS-based construction.

Max Pro. Rounds	Single Branch	Double Branches
1	2^{-1}	2^{-1}
2	2^{-3}	2^{-1}
3	2^{-5}	2^{-1}
4	2^{-7}	$2^{-5.4}$
5	2^{-7}	$2^{-7.3}$
6	$2^{-9.6}$	$2^{-11.1}$
7	$2^{-9.4}$	$2^{-12.5}$
8	2^{-11}	$2^{-12.5}$
9	2^{-12}	$2^{-12.5}$
10	$2^{-12.5}$	$2^{-12.5}$
11	$2^{-12.5}$	$2^{-12.5}$
12	$2^{-12.5}$	$2^{-12.5}$

For the GFS-based toy cipher, the maximal linear bias ($2^{-6.4}$) becomes stable in 9 rounds and 6 rounds for a single branch and double branches, respectively.

Summary. In our experiments, both the maximal differential probability and linear bias of the double branches reach a stable value in a smaller number of rounds than that of the single branch. Of course the scale of experiment is limited and a more theoretical support should be desired. However, these results suggest that the double branch enhances the security of the single branch. We also emphasize that the security of Orthros is never ensured based on such a simple simulation. Instead, a comprehensive study is performed.

B Detailed Explanations for Conditions 1 and 2

B.1 Condition 1

Fig 10 shows the transition of the state after applying P_{bk1}, which satisfies Condition 1. The state is represented as a 16×8 bit array, where S_0, S_1, S_2, S_3 are nibbles consisting of the first state column. Let us focus on the leftmost column. After applying a bit-permutation satisfying Condition 1, for $0 \leq i \leq 3$, Fig 10 shows that the 4 bits of S_i are mapped to different columns. The same applies to the remaining 7 columns.

B.2 Proof of Condition 2

For each active bit in the nibble cell S_i ($0 \leq i \leq 31$) in the input, after applying the S-box and the bit permutation satisfying Condition 1, there will exist 4

$$\begin{bmatrix} s_0 & s_{16} & s_{32} & s_{48} & s_{64} & s_{80} & s_{96} & s_{112} \\ s_1 & s_{17} & s_{33} & s_{49} & s_{65} & s_{81} & s_{97} & s_{113} \\ s_2 & s_{18} & s_{34} & s_{50} & s_{66} & s_{82} & s_{98} & s_{114} \\ s_3 & s_{19} & s_{35} & s_{51} & s_{67} & s_{83} & s_{99} & s_{115} \\ s_4 & s_{20} & s_{36} & s_{52} & s_{68} & s_{84} & s_{100} & s_{116} \\ s_5 & s_{21} & s_{37} & s_{53} & s_{69} & s_{85} & s_{101} & s_{117} \\ s_6 & s_{22} & s_{38} & s_{54} & s_{70} & s_{86} & s_{102} & s_{118} \\ s_7 & s_{23} & s_{39} & s_{55} & s_{71} & s_{87} & s_{103} & s_{119} \\ s_8 & s_{24} & s_{40} & s_{56} & s_{72} & s_{88} & s_{104} & s_{120} \\ s_9 & s_{25} & s_{41} & s_{57} & s_{73} & s_{89} & s_{105} & s_{121} \\ s_{10} & s_{26} & s_{42} & s_{58} & s_{74} & s_{90} & s_{106} & s_{122} \\ s_{11} & s_{27} & s_{43} & s_{59} & s_{75} & s_{91} & s_{107} & s_{123} \\ s_{12} & s_{28} & s_{44} & s_{60} & s_{76} & s_{92} & s_{108} & s_{124} \\ s_{13} & s_{29} & s_{45} & s_{61} & s_{77} & s_{93} & s_{109} & s_{125} \\ s_{14} & s_{30} & s_{46} & s_{62} & s_{78} & s_{94} & s_{110} & s_{126} \\ s_{15} & s_{31} & s_{47} & s_{63} & s_{79} & s_{95} & s_{111} & s_{127} \end{bmatrix} \xRightarrow{P_{bk1}} \begin{bmatrix} s_0 & s_{20} & s_{119} & s_7 & s_{79} & s_{53} & s_{126} & s_{19} \\ s_{11} & s_{57} & s_{26} & s_{107} & s_{30} & s_{93} & s_{59} & s_{104} \\ s_{58} & s_{63} & s_{95} & s_{74} & s_{25} & s_{44} & s_{91} & s_{56} \\ s_{29} & s_{35} & s_{81} & s_{41} & s_{13} & s_{27} & s_6 & s_{120} \\ s_{47} & s_{80} & s_9 & s_{92} & s_{86} & s_{90} & s_{121} & s_{88} \\ s_{36} & s_{89} & s_{39} & s_1 & s_{18} & s_{101} & s_{34} & s_{112} \\ s_{100} & s_4 & s_{40} & s_{16} & s_{48} & s_{122} & s_{110} & s_{78} \\ s_{49} & s_{106} & s_{113} & s_{109} & s_{123} & s_2 & s_{17} & s_{14} \\ s_{111} & s_{12} & s_{102} & s_{85} & s_{103} & s_{114} & s_{52} & s_{98} \\ s_{33} & s_{116} & s_{105} & s_{82} & s_3 & s_{38} & s_{96} & s_{46} \\ s_{83} & s_{115} & s_{50} & s_{37} & s_{99} & s_{77} & s_{43} & s_{23} \\ s_{73} & s_{97} & s_{67} & s_{69} & s_{55} & s_{87} & s_{61} & s_{32} \\ s_{76} & s_{42} & s_{125} & s_{127} & s_{45} & s_{51} & s_{10} & s_{84} \\ s_{68} & s_{70} & s_{54} & s_8 & s_{72} & s_{15} & s_{64} & s_{71} \\ s_{118} & s_{75} & s_{60} & s_{31} & s_{124} & s_{22} & s_{117} & s_{94} \\ s_{65} & s_{24} & s_{28} & s_{62} & s_{108} & s_5 & s_{21} & s_{66} \end{bmatrix}$$

$$S_0 = (s_0, s_1, s_2, s_3)^T \ S_1 = (s_4, s_5, s_6, s_7)^T \ S_2 = (s_8, s_9, s_{10}, s_{11})^T \ S_3 = (s_{12}, s_{13}, s_{14}, s_{15})^T$$

Fig. 10: Transition of a state after applying P_{bk1}.

different groups of inputs to the binary matrix, each of which will contain exactly one active nibble, as shown in Fig. 11. Therefore, there will be 12 active nibbles after MatrixMul in the first round, which will activate 12 nibbles located in the same positions in the second round after S-box operation, as depicted in Fig. 12. Therefore, there are 12 nibbles (48 bits in total) in the state after the S-box (with full-diffusion property) operation in the second round, independent of the value of the one active bit in the input to the first round.

After applying a permutation satisfying Condition 2 for these 48 bits, in each column of the 4 × 8 array, there exist at least 2 nibble cells containing the bits coming from these 48 bits, as shown in Fig. 13 for bit level and in Fig. 14 for nibble level. In other words, after applying the bit permutation satisfying Condition 2 in the second round, in each column of the nibble array, there are at least 2 nibbles dependent of the one active bit in the input to the first round. When the MatrixMul operation is further applied to each column of the 4 × 8 nibble array, the values of all the four nibbles in each column will therefore dependent of the one active bit in the input to the first round. However, it cannot be guaranteed that the value of each bit will be dependent of the one active bit. Thus, after further applying the S-box with a full-diffusion property in the third round, all 128 bits become dependent of the one active bit. This means that the full diffusion is achieved by 2.5 rounds.

An example to explain the 2.5-round diffusion can be referred to Fig. 11, 12, 13, and Fig. 14.

C Details of Security Evaluation

C.1 DDT of S-box

The aforementioned DDT table of our S-box is shown shown in Table 13 , where d_{in} and d_{out} denote the input and output difference of 4-bit S-box, respectively.

$$\begin{bmatrix} {\color{red}s_{0}} & s_{16} & s_{32} & s_{48} & s_{64} & s_{80} & s_{96} & s_{112} \\ {\color{red}s_{1}} & s_{17} & s_{33} & s_{49} & s_{65} & s_{81} & s_{97} & s_{113} \\ {\color{red}s_{2}} & s_{18} & s_{34} & s_{50} & s_{66} & s_{82} & s_{98} & s_{114} \\ {\color{red}s_{3}} & s_{19} & s_{35} & s_{51} & s_{67} & s_{83} & s_{99} & s_{115} \\ s_{4} & s_{20} & s_{36} & s_{52} & s_{68} & s_{84} & s_{100} & s_{116} \\ s_{5} & s_{21} & s_{37} & s_{53} & s_{69} & s_{85} & s_{101} & s_{117} \\ s_{6} & s_{22} & s_{38} & s_{54} & s_{70} & s_{86} & s_{102} & s_{118} \\ s_{7} & s_{23} & s_{39} & s_{55} & s_{71} & s_{87} & s_{103} & s_{119} \\ s_{8} & s_{24} & s_{40} & s_{56} & s_{72} & s_{88} & s_{104} & s_{120} \\ s_{9} & s_{25} & s_{41} & s_{57} & s_{73} & s_{89} & s_{105} & s_{121} \\ s_{10} & s_{26} & s_{42} & s_{58} & s_{74} & s_{90} & s_{106} & s_{122} \\ s_{11} & s_{27} & s_{43} & s_{59} & s_{75} & s_{91} & s_{107} & s_{123} \\ s_{12} & s_{28} & s_{44} & s_{60} & s_{76} & s_{92} & s_{108} & s_{124} \\ s_{13} & s_{29} & s_{45} & s_{61} & s_{77} & s_{93} & s_{109} & s_{125} \\ s_{14} & s_{30} & s_{46} & s_{62} & s_{78} & s_{94} & s_{110} & s_{126} \\ s_{15} & s_{31} & s_{47} & s_{63} & s_{79} & s_{95} & s_{111} & s_{127} \end{bmatrix} \overset{P_{bk1}}{\Longrightarrow} \begin{bmatrix} {\color{red}s_{0}} & s_{20} & s_{119} & s_{7} & s_{79} & s_{53} & s_{126} & s_{19} \\ s_{11} & s_{57} & s_{26} & s_{107} & s_{30} & s_{93} & s_{59} & s_{104} \\ s_{58} & s_{63} & s_{95} & s_{74} & s_{25} & s_{44} & s_{91} & s_{56} \\ s_{29} & s_{35} & s_{81} & s_{41} & s_{13} & s_{27} & s_{6} & s_{120} \\ s_{47} & s_{80} & s_{9} & s_{92} & s_{86} & s_{90} & s_{121} & s_{88} \\ s_{36} & s_{89} & s_{39} & {\color{red}s_{1}} & s_{18} & s_{101} & s_{34} & s_{112} \\ s_{100} & s_{4} & s_{40} & s_{16} & s_{48} & s_{122} & s_{110} & s_{78} \\ s_{49} & s_{106} & s_{113} & s_{109} & s_{123} & {\color{red}s_{2}} & s_{17} & s_{14} \\ s_{111} & s_{12} & s_{102} & s_{85} & s_{103} & s_{114} & s_{52} & s_{98} \\ s_{33} & s_{116} & s_{105} & s_{82} & {\color{red}s_{3}} & s_{38} & s_{96} & s_{46} \\ s_{83} & s_{115} & s_{50} & s_{37} & s_{99} & s_{77} & s_{43} & s_{23} \\ s_{73} & s_{97} & s_{67} & s_{69} & s_{55} & s_{87} & s_{61} & s_{32} \\ s_{76} & s_{42} & s_{125} & s_{127} & s_{45} & s_{51} & s_{10} & s_{84} \\ s_{68} & s_{70} & s_{54} & s_{8} & s_{72} & s_{15} & s_{64} & s_{71} \\ s_{118} & s_{75} & s_{60} & s_{31} & s_{124} & s_{22} & s_{117} & s_{94} \\ s_{65} & s_{24} & s_{28} & s_{62} & s_{108} & s_{5} & s_{21} & s_{66} \end{bmatrix}$$

$${\color{red}S_0 = (s_0, s_1, s_2, s_3)^T}$$

Fig. 11: The 4 active bits after the bit permutation in the first round, as marked in red.

$$\begin{bmatrix} S_0 & S_4 & S_8 & {\color{red}S_{12}} & {\color{red}S_{16}} & {\color{red}S_{20}} & S_{24} & S_{28} \\ {\color{red}S_1} & S_5 & S_9 & S_{13} & {\color{red}S_{17}} & S_{21} & S_{25} & S_{29} \\ {\color{red}S_2} & S_6 & S_{10} & {\color{red}S_{14}} & S_{18} & {\color{red}S_{22}} & S_{26} & S_{30} \\ {\color{red}S_3} & S_7 & S_{11} & {\color{red}S_{15}} & {\color{red}S_{19}} & {\color{red}S_{23}} & S_{27} & S_{31} \end{bmatrix}$$

Fig. 12: The 12 active nibbles after MatrixMul in the first round, marked in red.

$$\begin{bmatrix} s_{0} & s_{16} & s_{32} & {\color{red}s_{48}} & {\color{red}s_{64}} & {\color{red}s_{80}} & s_{96} & s_{112} \\ s_{1} & s_{17} & s_{33} & {\color{red}s_{49}} & {\color{red}s_{65}} & {\color{red}s_{81}} & s_{97} & s_{113} \\ s_{2} & s_{18} & s_{34} & {\color{red}s_{50}} & {\color{red}s_{66}} & {\color{red}s_{82}} & s_{98} & s_{114} \\ s_{3} & s_{19} & s_{35} & {\color{red}s_{51}} & {\color{red}s_{67}} & {\color{red}s_{83}} & s_{99} & s_{115} \\ {\color{red}s_{4}} & s_{20} & s_{36} & s_{52} & {\color{red}s_{68}} & s_{84} & s_{100} & s_{116} \\ {\color{red}s_{5}} & s_{21} & s_{37} & s_{53} & {\color{red}s_{69}} & s_{85} & s_{101} & s_{117} \\ {\color{red}s_{6}} & s_{22} & s_{38} & s_{54} & {\color{red}s_{70}} & s_{86} & s_{102} & s_{118} \\ {\color{red}s_{7}} & s_{23} & s_{39} & s_{55} & {\color{red}s_{71}} & s_{87} & s_{103} & s_{119} \\ {\color{red}s_{8}} & s_{24} & s_{40} & {\color{red}s_{56}} & s_{72} & {\color{red}s_{88}} & s_{104} & s_{120} \\ {\color{red}s_{9}} & s_{25} & s_{41} & {\color{red}s_{57}} & s_{73} & {\color{red}s_{89}} & s_{105} & s_{121} \\ {\color{red}s_{10}} & s_{26} & s_{42} & {\color{red}s_{58}} & s_{74} & {\color{red}s_{90}} & s_{106} & s_{122} \\ {\color{red}s_{11}} & s_{27} & s_{43} & {\color{red}s_{59}} & s_{75} & {\color{red}s_{91}} & s_{107} & s_{123} \\ {\color{red}s_{12}} & s_{28} & s_{44} & {\color{red}s_{60}} & {\color{red}s_{76}} & {\color{red}s_{92}} & s_{108} & s_{124} \\ {\color{red}s_{13}} & s_{29} & s_{45} & {\color{red}s_{61}} & {\color{red}s_{77}} & {\color{red}s_{93}} & s_{109} & s_{125} \\ {\color{red}s_{14}} & s_{30} & s_{46} & {\color{red}s_{62}} & {\color{red}s_{78}} & {\color{red}s_{94}} & s_{110} & s_{126} \\ {\color{red}s_{15}} & s_{31} & s_{47} & {\color{red}s_{63}} & {\color{red}s_{79}} & {\color{red}s_{95}} & s_{111} & s_{127} \end{bmatrix} \overset{P_{bk1}}{\Longrightarrow} \begin{bmatrix} s_{0} & s_{20} & s_{119} & {\color{red}s_{7}} & {\color{red}s_{79}} & s_{53} & s_{126} & s_{19} \\ {\color{red}s_{11}} & {\color{red}s_{57}} & s_{26} & s_{107} & s_{30} & {\color{red}s_{93}} & {\color{red}s_{59}} & s_{104} \\ {\color{red}s_{58}} & {\color{red}s_{63}} & {\color{red}s_{95}} & s_{74} & s_{25} & s_{44} & {\color{red}s_{91}} & {\color{red}s_{56}} \\ s_{29} & s_{35} & {\color{red}s_{81}} & s_{41} & {\color{red}s_{13}} & s_{27} & {\color{red}s_{6}} & s_{120} \\ s_{47} & {\color{red}s_{80}} & {\color{red}s_{9}} & {\color{red}s_{92}} & s_{86} & {\color{red}s_{90}} & s_{121} & {\color{red}s_{88}} \\ s_{36} & {\color{red}s_{89}} & s_{39} & s_{1} & s_{18} & s_{101} & s_{34} & s_{112} \\ s_{100} & {\color{red}s_{4}} & s_{40} & s_{16} & {\color{red}s_{48}} & s_{122} & s_{110} & {\color{red}s_{78}} \\ {\color{red}s_{49}} & s_{106} & s_{113} & s_{109} & s_{123} & s_{2} & s_{17} & {\color{red}s_{14}} \\ s_{111} & {\color{red}s_{12}} & s_{102} & s_{85} & s_{103} & s_{114} & s_{52} & s_{98} \\ s_{33} & s_{116} & s_{105} & {\color{red}s_{82}} & s_{3} & s_{38} & s_{96} & s_{46} \\ {\color{red}s_{83}} & s_{115} & {\color{red}s_{50}} & s_{37} & s_{99} & {\color{red}s_{77}} & s_{43} & s_{23} \\ s_{73} & s_{97} & {\color{red}s_{67}} & {\color{red}s_{69}} & s_{55} & s_{87} & {\color{red}s_{61}} & s_{32} \\ {\color{red}s_{76}} & s_{42} & s_{125} & s_{127} & s_{45} & {\color{red}s_{51}} & {\color{red}s_{10}} & s_{84} \\ {\color{red}s_{68}} & {\color{red}s_{70}} & s_{54} & {\color{red}s_{8}} & s_{72} & {\color{red}s_{15}} & {\color{red}s_{64}} & {\color{red}s_{71}} \\ s_{118} & s_{75} & {\color{red}s_{60}} & s_{31} & s_{124} & s_{22} & s_{117} & {\color{red}s_{94}} \\ {\color{red}s_{65}} & s_{24} & s_{28} & {\color{red}s_{62}} & s_{108} & {\color{red}s_{5}} & s_{21} & {\color{red}s_{66}} \end{bmatrix}$$

Fig. 13: The 48 active bits after bit permutation in the second round, marked in red.

$$\begin{bmatrix} {\color{red}S_0} & {\color{red}S_4} & {\color{red}S_8} & {\color{red}S_{12}} & {\color{red}S_{16}} & {\color{red}S_{20}} & {\color{red}S_{24}} & {\color{red}S_{28}} \\ {\color{red}S_1} & {\color{red}S_5} & {\color{red}S_9} & {\color{red}S_{13}} & {\color{red}S_{17}} & {\color{red}S_{21}} & {\color{red}S_{25}} & {\color{red}S_{29}} \\ {\color{red}S_2} & {\color{red}S_6} & {\color{red}S_{10}} & {\color{red}S_{14}} & S_{18} & {\color{red}S_{22}} & S_{26} & S_{30} \\ {\color{red}S_3} & {\color{red}S_7} & {\color{red}S_{11}} & {\color{red}S_{15}} & S_{19} & {\color{red}S_{23}} & {\color{red}S_{27}} & {\color{red}S_{31}} \end{bmatrix}$$

Fig. 14: The active nibbles after bit permutation in the second round, marked in red.

Table 13: The differential distribution table of S-box.

d_{out} d_{in}	0x0	0x1	0x2	0x3	0x4	0x5	0x6	0x7	0x8	0x9	0xa	0xb	0xc	0xd	0xe	0xf
0x0	16	0	0	0	0	0	0	0	0	0	0	0	0	0	0	0
0x1	0	2	2	4	0	2	2	0	0	0	0	4	0	0	0	0
0x2	0	0	2	2	4	4	0	0	2	2	0	0	0	0	0	0
0x3	0	2	2	0	0	2	0	2	0	0	2	2	0	0	4	0
0x4	0	0	2	0	2	0	4	0	2	2	0	2	2	0	0	0
0x5	0	0	2	2	0	4	0	0	0	4	0	0	0	0	2	2
0x6	0	2	2	0	2	0	0	2	0	0	0	0	2	2	2	2
0x7	0	2	0	0	0	0	2	4	0	0	2	0	4	2	0	0
0x8	0	2	0	0	2	0	0	0	4	2	4	0	2	0	0	0
0x9	0	0	0	2	0	0	0	2	0	2	2	2	2	0	0	4
0xa	0	2	0	0	2	0	0	0	0	2	2	2	0	2	4	0
0xb	0	0	2	0	0	0	2	0	2	0	2	2	0	2	0	4
0xc	0	2	2	2	0	2	0	0	0	0	2	0	2	2	2	0
0xd	0	2	0	2	0	0	2	2	2	2	0	0	0	2	0	2
0xe	0	0	0	0	0	2	4	2	4	0	0	0	0	2	0	2
0xf	0	0	0	2	4	0	0	2	0	0	0	2	2	2	2	0

C.2 Modeling S-box

Based on the method of [SHW+14], we derive following 37 linear inequalities from Table 13, where $d_{in} = (d_{in_0}, d_{in_1}, d_{in_2}, d_{in_3})$ and $d_{out} = (d_{out_0}, d_{out_1}, d_{out_2}, d_{out_3})$.

$$\begin{cases}
-d_{in_0} - d_{in_1} + 2d_{in_2} - d_{in_3} - 2d_{out_0} + 2d_{out_1} - d_{out_2} + d_{out_3} + 3 & \geq 0 \\
d_{in_0} + d_{in_1} - d_{in_2} + d_{in_3} + d_{out_0} + d_{out_1} + d_{out_2} & \geq 0 \\
d_{in_0} + 2d_{in_2} + d_{in_3} + d_{out_0} - d_{out_1} - d_{out_2} - 2d_{out_3} + 2 & \geq 0 \\
2d_{in_0} - d_{in_1} + d_{in_2} + 2d_{in_3} + d_{out_0} - d_{out_1} + d_{out_2} - 2d_{out_3} + 2 & \geq 0 \\
d_{in_0} - 2d_{in_1} - 2d_{in_2} - d_{in_3} + 2d_{out_0} - 2d_{out_1} + 2d_{out_2} - d_{out_3} + 6 & \geq 0 \\
-d_{in_0} + 2d_{in_1} - 2d_{in_2} - d_{in_3} + 2d_{out_0} + d_{out_1} - d_{out_2} - 2d_{out_3} + 5 & \geq 0 \\
d_{in_0} + d_{in_1} + 2d_{in_2} + 2d_{in_3} - d_{out_1} - d_{out_3} & \geq 0 \\
d_{in_0} + 2d_{in_1} + d_{in_2} + 2d_{in_3} - d_{out_0} - d_{out_1} - d_{out_2} - d_{out_3} + 1 & \geq 0 \\
d_{in_0} + d_{in_1} - d_{in_2} + d_{out_0} - d_{out_1} - d_{out_2} + d_{out_3} + 2 & \geq 0 \\
d_{in_1} + d_{in_2} + 2d_{in_3} - d_{out_1} - d_{out_2} - d_{out_3} + 1 & \geq 0 \\
2d_{in_0} + d_{in_2} + d_{in_3} - 2d_{out_0} + d_{out_1} - 2d_{out_2} + 2d_{out_3} + 2 & \geq 0 \\
d_{in_0} - d_{in_2} - d_{in_3} - d_{out_0} - d_{out_1} - d_{out_2} - d_{out_3} + 5 & \geq 0 \\
d_{in_0} + 2d_{in_1} + 2d_{in_2} - 2d_{out_0} - 1d_{out_1} - 1d_{out_2} + d_{out_3} + 2 & \geq 0 \\
-d_{in_0} + 2d_{in_1} + d_{in_2} + d_{in_3} + 2d_{out_0} - 2d_{out_2} + d_{out_3} + 1 & \geq 0 \\
d_{in_0} + d_{in_1} + d_{in_2} - d_{in_3} - d_{out_0} + d_{out_1} + d_{out_2} + d_{out_3} & \geq 0 \\
d_{in_0} + d_{in_1} + d_{in_2} - 2d_{out_0} - d_{out_1} + d_{out_2} - d_{out_3} + 2 & \geq 0 \\
-d_{in_0} + d_{in_1} + d_{in_3} + d_{out_0} - d_{out_1} - d_{out_3} + 2 & \geq 0 \\
-d_{in_0} - d_{in_1} + d_{in_2} - d_{out_0} + d_{out_1} - d_{out_2} - d_{out_3} + 4 & \geq 0 \\
d_{in_0} - d_{in_2} + d_{in_3} + d_{out_0} - d_{out_1} - d_{out_2} + d_{out_3} + 2 & \geq 0 \\
d_{in_0} - d_{in_1} - d_{in_2} + d_{out_1} - d_{out_2} - d_{out_3} + 3 & \geq 0 \\
-d_{in_1} - 2d_{in_2} - d_{in_3} - 2d_{out_0} + 2d_{out_1} + 2d_{out_2} - d_{out_3} + 5 & \geq 0 \\
-3d_{in_0} - 2d_{in_1} - 3d_{in_2} + d_{in_3} + 4d_{out_0} + 3d_{out_1} + d_{out_2} + 2d_{out_3} + 4 & \geq 0 \\
2d_{in_0} - d_{in_1} + d_{in_2} - 3d_{in_3} + 2d_{out_0} + d_{out_1} + 4d_{out_2} + 3d_{out_3} & \geq 0 \\
d_{in_0} - 2d_{in_1} - 2d_{in_2} - 2d_{out_0} + 2d_{out_1} + d_{out_2} - 1d_{out_3} + 5 & \geq 0 \\
-3d_{in_0} + d_{in_1} + d_{in_2} - 2d_{in_3} + 2d_{out_0} - 2d_{out_1} + 3d_{out_2} - 1d_{out_3} + 5 & \geq 0 \\
-2d_{in_0} - 2d_{in_1} + d_{in_2} + d_{in_3} + 3d_{out_0} + 2d_{out_1} + 4d_{out_2} + 4d_{out_3} & \geq 0 \\
d_{in_0} - d_{in_1} + 2d_{in_2} - 3d_{in_3} + d_{out_0} - d_{out_1} + 2d_{out_2} + 3d_{out_3} + 2 & \geq 0 \\
-d_{in_0} + d_{in_1} - 2d_{in_2} + d_{in_3} - 2d_{out_0} - d_{out_1} + 2d_{out_2} + 2d_{out_3} + 4 & \geq 0 \\
-2d_{in_0} - 2d_{in_1} + d_{in_2} + d_{in_3} + 2d_{out_0} - 1d_{out_1} + d_{out_2} + 2d_{out_3} + 3 & \geq 0 \\
-d_{in_0} - 2d_{in_1} - d_{in_2} + d_{in_3} - d_{out_0} + 2d_{out_1} + d_{out_2} - 2d_{out_3} + 5 & \geq 0 \\
d_{in_1} - d_{in_2} - d_{out_0} - d_{out_1} + d_{out_2} + d_{out_3} + 2 & \geq 0 \\
-d_{in_0} - d_{in_1} - d_{in_2} + d_{in_3} - d_{out_0} - d_{out_2} + d_{out_3} + 4 & \geq 0 \\
-3d_{in_0} - 4d_{in_1} - 2d_{in_2} - 2d_{in_3} + d_{out_0} + 3d_{out_1} - d_{out_2} + 4d_{out_3} + 8 & \geq 0 \\
-d_{in_1} - d_{in_2} - d_{in_3} - d_{out_0} - d_{out_1} - d_{out_2} - d_{out_3} + 6 & \geq 0 \\
-d_{in_0} + d_{in_1} - d_{in_3} - d_{out_0} - d_{out_1} - d_{out_2} + d_{out_3} + 4 & \geq 0 \\
d_{in_0} - d_{in_1} - d_{in_2} - d_{in_3} - d_{out_0} - d_{out_1} - d_{out_2} + 5 & \geq 0 \\
-d_{in_0} + d_{in_2} - d_{in_3} - d_{out_0} - d_{out_1} - d_{out_2} + d_{out_3} + 4 & \geq 0
\end{cases}$$

C.3 Impossible Differential Characteristics of **Orthros**/Branch1/Branch2

3/5/5-round impossible differential characteristics of Orthros/Branch1/Branch2 are shown as follows.

$$\text{Orthros}: \overset{\text{Input}}{\begin{bmatrix} 0&0&0&0&0&0&0&0 \\ 0&0&0&0&0&0&0&0 \\ 0&0&0&0&0&0&0&0 \\ 0&0&0&0&0&0&0&0 \\ 1&0&0&0&0&0&0&0 \\ 0&0&0&0&0&0&0&0 \\ 0&0&0&0&0&0&0&0 \\ 0&0&0&0&0&0&0&0 \\ 0&0&0&0&0&0&0&0 \\ 0&0&0&0&0&0&0&0 \\ 0&0&0&0&0&0&0&0 \\ 0&0&0&0&0&0&0&0 \\ 0&0&0&0&0&0&0&0 \\ 0&0&0&0&0&0&0&0 \\ 0&0&0&0&0&0&0&0 \\ 0&0&0&0&0&0&0&0 \end{bmatrix}} \xrightarrow{3 \text{ rounds}} \overset{\text{Output}}{\begin{bmatrix} 0&0&0&0&0&0&1&0 \\ 0&0&0&0&0&0&0&0 \\ 0&0&0&0&0&0&0&0 \\ 0&0&0&0&0&0&0&0 \\ 0&0&0&0&0&0&0&0 \\ 0&0&0&0&0&0&0&0 \\ 0&0&0&0&0&0&0&0 \\ 0&0&0&0&0&0&0&0 \\ 0&0&0&0&0&0&0&0 \\ 0&0&0&0&0&0&0&0 \\ 0&0&0&0&0&0&0&0 \\ 0&0&0&0&0&0&0&0 \\ 0&0&0&0&0&0&0&0 \\ 0&0&0&0&0&0&0&0 \\ 0&0&0&0&0&0&0&0 \\ 0&0&0&0&0&0&0&0 \end{bmatrix}},$$

$$\text{Branch1}: \overset{\text{Input}}{\begin{bmatrix} 0&0&0&0&0&0&0&0 \\ 0&0&0&0&0&0&0&0 \\ 1&0&0&0&0&0&0&0 \\ 0&0&0&0&0&0&0&0 \\ 0&0&0&0&0&0&0&0 \\ 0&0&0&0&0&0&0&0 \\ 0&0&0&0&0&0&0&0 \\ 0&0&0&0&0&0&0&0 \\ 0&0&0&0&0&0&0&0 \\ 0&0&0&0&0&0&0&0 \\ 0&0&0&0&0&0&0&0 \\ 0&0&0&0&0&0&0&0 \\ 0&0&0&0&0&0&0&0 \\ 0&0&0&0&0&0&0&0 \\ 0&0&0&0&0&0&0&0 \\ 0&0&0&0&0&0&0&0 \end{bmatrix}} \xrightarrow{5 \text{ rounds}} \overset{\text{Output}}{\begin{bmatrix} 0&0&0&0&0&0&0&1 \\ 0&0&0&0&0&0&0&0 \\ 0&0&0&0&0&0&0&0 \\ 0&0&0&0&0&0&0&0 \\ 0&0&0&0&0&0&0&0 \\ 0&0&0&0&0&0&0&0 \\ 0&0&0&0&0&0&0&0 \\ 0&0&0&0&0&0&0&0 \\ 0&0&0&0&0&0&0&0 \\ 0&0&0&0&0&0&0&0 \\ 0&0&0&0&0&0&0&0 \\ 0&0&0&0&0&0&0&0 \\ 0&0&0&0&0&0&0&0 \\ 0&0&0&0&0&0&0&0 \\ 0&0&0&0&0&0&0&0 \\ 0&0&0&0&0&0&0&0 \end{bmatrix}},$$

$$\text{Branch2}: \overset{\text{Input}}{\begin{bmatrix} 1&0&0&0&0&0&0&0 \\ 0&0&0&0&0&0&0&0 \\ 0&0&0&0&0&0&0&0 \\ 0&0&0&0&0&0&0&0 \\ 0&0&0&0&0&0&0&0 \\ 0&0&0&0&0&0&0&0 \\ 0&0&0&0&0&0&0&0 \\ 0&0&0&0&0&0&0&0 \\ 0&0&0&0&0&0&0&0 \\ 0&0&0&0&0&0&0&0 \\ 0&0&0&0&0&0&0&0 \\ 0&0&0&0&0&0&0&0 \\ 0&0&0&0&0&0&0&0 \\ 0&0&0&0&0&0&0&0 \\ 0&0&0&0&0&0&0&0 \\ 0&0&0&0&0&0&0&0 \end{bmatrix}} \xrightarrow{5 \text{ rounds}} \overset{\text{Output}}{\begin{bmatrix} 0&0&0&0&0&0&0&0 \\ 0&0&0&0&0&0&0&0 \\ 0&0&0&0&0&0&0&0 \\ 0&0&0&0&0&0&0&0 \\ 0&0&0&0&0&0&0&0 \\ 0&0&0&0&0&0&0&0 \\ 0&0&0&0&0&0&0&0 \\ 1&0&0&0&0&0&0&0 \\ 0&0&0&0&0&0&0&0 \\ 0&0&0&0&0&0&0&0 \\ 0&0&0&0&0&0&0&0 \\ 0&0&0&0&0&0&0&0 \\ 0&0&0&0&0&0&0&0 \\ 0&0&0&0&0&0&0&0 \\ 0&0&0&0&0&0&0&0 \\ 0&0&0&0&0&0&0&0 \end{bmatrix}}.$$

C.4 Modeling for Division Property

Modeling S-box. Similar to Section 4.2, one could build a table to describe the propagation of the division property through `S-box`, as shown in Table 14. In this

Table 14: The propagation of the division property for the S-box.

v u	0x0	0x1	0x2	0x4	0x8	0x3	0x5	0x9	0x6	0xa	0xc	0x7	0xb	0xd	0xe	0xf
0x0	*	*	*	*	*	*	*	*	*	*	*	*	*	*	*	*
0x1		*	*	*	*	*	*	*	*	*	*	*	*	*	*	*
0x2		*	*	*	*	*	*	*	*	*	*	*	*	*	*	*
0x4		*	*	*	*	*	*	*	*	*	*	*	*	*	*	*
0x8		*	*	*	*	*	*	*	*	*	*	*	*	*	*	*
0x3		*	*	*		*	*	*	*	*	*	*	*	*	*	*
0x5		*	*	*	*	*	*	*	*	*	*	*	*	*	*	*
0x9		*	*		*	*	*	*	*	*	*	*	*	*	*	*
0x6		*	*	*	*	*	*	*	*	*	*	*	*	*	*	*
0xa		*		*	*	*	*	*	*	*	*	*	*	*	*	*
0xc			*	*	*	*	*	*	*	*	*	*	*	*	*	*
0x7		*	*	*		*	*	*	*	*	*	*	*	*	*	*
0xb		*				*	*	*	*	*	*	*	*	*	*	*
0xd			*		*	*	*	*	*	*	*	*	*	*	*	*
0xe				*	*		*	*	*	*	*	*	*	*	*	*
0xf																*

table, u and v denote the input and output division property of `S-box`, respectively. The entry at (u, v) is $*$ when the propagation $u \to v$ is possible. Otherwise, the propagation is impossible. Based on the method proposed by [SHW$^+$14], such a table is equivalent to the linear inequalities as shown below, where $u = (u_0, u_1, u_2, u_3)$ and $v = (v_0, v_1, v_2, v_3)$.

$$\begin{cases} -u_0 - u_1 + 2v_0 + 2v_1 + 2v_2 + v_3 & \geq 0 \\ -u_0 - u_2 + v_0 + v_1 + v_3 + 1 & \geq 0 \\ -u_2 - u_3 + v_0 + 2v_1 + 2v_2 + 2v_3 & \geq 0 \\ -u_0 - u_1 - u_3 + 3v_0 + 2v_1 + 3v_2 + 2v_3 & \geq 0 \\ -u_0 - u_3 + 2v_0 + v_1 + 2v_2 + 2v_3 & \geq 0 \\ -u_0 - u_1 - u_2 + v_0 + v_1 + 2 & \geq 0 \\ -4u_0 - 3u_1 - 4u_2 - 4u_3 + v_0 + v_1 + v_2 + 2v_3 + 10 & \geq 0 \end{cases}$$

Modeling the Binary Matrix. For the `matrixMul` operation, it can also be viewed that the binary matrix M_b works on four bits independently. Let $B = M_b \cdot A$, where $A, B \in \mathbb{F}_2^4$. Therefore, we could pre-compute a table to describe the mapping from A to B, as specified in Table 15.

Table 15: The mapping of the binary matrix.

A	0	1	2	3	4	5	6	7	8	9	a	b	c	d	e	f
B	0	14	13	3	11	5	6	8	7	9	10	4	12	2	1	15

To model the propagation of the division property through the binary matrix, similar to the way we model `S-box`, we first build a table to describe the propagation rule (Table 16), where w and z denote the input and output division property. The entroy (w, z) is marked as $*$ when the propagation $w \rightarrow z$ is possible. Otherwise, the propagation is impossible. By using the method of [SHW⁺14],

Table 16: The propagation of the division property for the binary matrix.

$w \backslash z$	0x0	0x1	0x2	0x4	0x8	0x3	0x5	0x9	0x6	0xa	0xc	0x7	0xb	0xd	0xe	0xf
0x0	*	*	*	*	*	*	*	*	*	*	*	*	*	*	*	*
0x1			*	*	*	*	*	*	*	*	*	*	*	*	*	*
0x2		*		*	*	*	*	*	*	*	*	*	*	*	*	*
0x4		*	*		*	*	*	*	*	*	*	*	*	*	*	*
0x8		*	*	*		*	*	*	*	*	*	*	*	*	*	*
0x3						*	*	*	*	*		*	*	*	*	*
0x5						*	*	*	*		*	*	*	*	*	*
0x9						*	*	*		*	*	*	*	*	*	*
0x6						*	*		*	*	*	*	*	*	*	*
0xa						*		*	*	*	*	*	*	*	*	*
0xc							*	*	*	*	*	*	*	*	*	*
0x7													*	*	*	*
0xb												*		*	*	*
0xd												*	*		*	*
0xe												*	*	*		*
0xf																*

Table 16 can be expressed by the linear inequalities as displayed below, where $w = (w_0, w_1, w_2, w_3)$ and $z = (z_0, z_1, z_2, z_3)$.

$$\begin{cases}
-w_0 - w_1 - w_2 + z_3 + 2 & \geq 0 \\
-w_0 - w_1 - w_3 + z_2 + 2 & \geq 0 \\
-w_0 - w_1 - w_2 - w_3 + z_0 + z_1 + z_2 + z_3 & \geq 0 \\
-w_0 - w_2 - w_3 + z_1 + 2 & \geq 0 \\
-w_1 - w_2 - w_3 + z_0 + 2 & \geq 0 \\
-w_0 - w_2 + z_0 + z_2 + 1 & \geq 0 \\
-w_0 - w_1 + z_0 + z_1 + 1 & \geq 0 \\
-w_1 - w_2 + z_1 + z_2 + 1 & \geq 0 \\
-w_1 - w_3 + z_1 + z_3 + 1 & \geq 0 \\
-w_2 + z_0 + z_1 + z_3 & \geq 0 \\
-w_3 + z_0 + z_1 + z_2 & \geq 0 \\
-w_2 - w_3 + z_2 + z_3 + 1 & \geq 0 \\
-w_1 + z_0 + z_2 + z_3 & \geq 0 \\
-w_0 + z_1 + z_2 + z_3 & \geq 0 \\
-w_0 - w_3 + z_0 + z_3 + 1 & \geq 0
\end{cases}$$

D Additional Hardware Results

Cipher	Area		Power	Energy	Latency	Max TP
	(μm^2)	(GE)	(mW)	(pJ)	(ps)	(Gbps)
Orthros	5766.1	29328	2.332	233.18	485.72	245.428
	5792.8	29464	2.187	218.74	450.00	264.910
	6013.5	30586	2.038	203.85	400.00	298.023
	7439.2	37838	2.637	263.73	351.55	339.096
Midori-128	5102.3	25952	3.354	335.36	850.55	140.156
	5116.7	26025	3.251	325.12	800.00	149.012
	5156.9	26229	3.132	313.15	750.00	158.946
	5298.5	26950	3.138	313.80	700.00	170.299
	5731.8	29153	3.305	330.49	650.00	183.399
	6976.4	35484	4.466	446.60	603.78	197.438
QARMA$_9$-128-σ_0	6263.3	31857	4.160	415.98	908.09	131.275
	6304.8	32068	3.810	380.95	800.00	149.012
	7085.8	36040	3.861	386.12	700.00	170.299
	8869.9	45115	5.611	561.05	640.00	186.265
PRINCE	1664.3	8465	0.671	67.14	536.37	222.252
	1671.5	8502	0.657	65.71	500.00	238.419
	1698.5	8639	0.604	60.36	450.00	264.910
	1889.6	9611	0.599	59.98	400.00	298.023
	2337.9	11891	0.894	89.43	371.62	320.783
Kangaroo12-PRF[1600]	26957.8	137114	13.470	1347.04	722.32	165.036
	27298.5	138847	12.223	1222.25	650.00	183.400
	28803.4	146502	12.884	1288.39	600.00	198.682
	31052.8	157943	13.096	1309.60	576.65	206.727
Kangaroo12-PRF[400]	7332.0	37293	3.812	381.22	765.95	155.636
	7407.3	37675	3.711	371.08	700.00	170.300
	7584.7	38578	3.501	350.11	650.00	183.400
	8278.4	42106	5.571	557.07	602.81	197.756
Subterranean-PRF	7582.4	38566	3.548	354.78	692.84	172.059
	7586.4	38586	3.385	338.53	650.00	183.400
	7661.4	38968	3.122	312.22	600.00	198.682
	8392.3	42865	2.878	287.80	543.21	219.453

Table 17: Results for the Nangate 15nm library. Power measured at 10 MHz.

Cipher	Area		Power	Energy	Latency	Max TP
	(μm^2)	(GE)	(mW)	(pJ)	(ns)	(Gbps)
Orthros	76712.1	27179	2.452	245.22	9.37	12.722
	77355.6	27407	2.525	252.49	8.00	14.901
	83566.3	29607	3.478	347.79	7.00	17.030
	95896.7	33976	4.447	444.73	6.00	19.868
	124746.6	44197	5.393	539.28	5.29	22.535
Midori-128	67710.8	23990	3.817	381.72	15.89	7.502
	67938.7	24070	4.090	408.97	14.00	8.515
	73455.8	26025	5.374	537.38	12.00	9.934
	90043.0	31902	7.200	719.96	10.00	11.921
	122156.3	43279	9.138	913.82	9.05	13.172
QARMA$_9$-128-σ_0	80258.5	28435	4.2252	422.52	17.40	6.851
	80844.1	28643	5.2578	525.78	15.00	7.947
	89048.8	31550	6.8206	682.06	13.00	9.170
	107814.3	38198	8.4356	843.56	11.00	10.837
	153286.0	54309	10.3168	1031.68	9.43	12.641
PRINCE	22036.6	7807	0.699	69.94	9.79	12.177
	22674.5	8033	0.911	91.09	8.00	14.901
	25879.3	9169	1.135	113.47	7.00	17.030
	31206.6	11056	1.421	142.12	6.00	19.868
	42518.8	15064	1.898	189.81	5.52	21.596
Kangaroo12-PRF[1600]	372818.5	132088	21.558	2155.83	16.21	7.354
	379806.1	134564	20.788	2078.78	14.00	8.515
	424274.4	150319	24.212	2421.24	11.00	10.837
	504947.1	178901	29.376	2937.59	9.12	13.071
Kangaroo12-PRF[400]	104761.8	37117	5.259	525.93	15.15	7.869
	104882.5	37159	5.661	566.09	14.00	8.515
	121185.4	42935	7.248	724.75	11.00	10.837
	151044.3	53514	9.119	911.92	9.27	12.860
Subterranean-PRF	103337.2	36612	3.367	336.72	14.28	8.348
	105067.4	37225	3.388	338.77	12.00	9.934
	123273.3	43675	5.149	514.85	10.00	11.921
	156786.4	55549	5.227	522.74	7.98	14.938

Table 18: Results for the TSMC 90nm library. Power measured at 10 MHz.

Cipher	Area		Power	Energy	Latency	Max TP
	(μm^2)	(GE)	(mW)	(pJ)	(ns)	(Gbps)
Orthros	21404.5	26756	15.952	1595.20	3.81	31.289
	21466.2	26833	14.858	1485.80	3.50	34.060
	21548.4	26936	13.386	1338.60	3.00	39.736
	24028.6	30036	13.237	1323.70	2.68	44.481
Midori-128	18784.7	23481	23.088	2308.79	6.29	18.952
	18808.6	23511	22.071	2207.10	6.00	19.868
	18971.7	23715	21.533	2153.30	5.50	21.674
	19666.7	24583	21.014	2101.40	5.00	23.842
	20396.6	25496	21.066	2106.60	4.72	25.256
QARMA$_9$-128-σ_0	22866.4	28583	28.055	2805.50	6.68	17.846
	22903.4	28629	27.896	2789.60	6.50	18.340
	22956.6	28696	25.678	2567.80	6.00	19.868
	23044.9	28806	23.804	2380.4	5.50	21.674
	24699.2	30874	24.174	2417.40	4.92	23.842
PRINCE	6037.4	7547	4.371	437.11	3.87	30.803
	6072.8	7591	4.135	413.54	3.50	34.060
	6473.9	8092	3.994	399.43	3.00	39.736
	6693.1	8366	4.005	400.55	2.92	40.825
Kangaroo12-PRF[1600]	99007.3	124069	85.880	8588.00	5.08	23.466
	101193.1	126808	82.437	8243.70	4.70	25.364
	100167.0	125522	79.505	7950.50	4.50	26.491
	102999.7	129072	78.764	7876.40	4.34	27.468
Kangaroo12-PRF[400]	26726.0	33491	24.496	2449.60	5.49	21.714
	26756.7	33530	23.986	2398.60	5.20	22.925
	27033.3	33876	22.812	2281.20	4.80	24.835
	27699.4	34711	21.814	2181.40	4.50	26.491
Subterranean-PRF	27671.7	34676	22.760	2276.03	5.01	23.794
	27696.2	34707	22.225	2222.50	4.70	25.364
	28071.5	35177	21.406	2140.60	4.30	27.723
	28960.2	36291	20.762	2076.20	3.98	29.952

Table 19: Results for the Nangate 45nm library. Power measured at 10 MHz.

E Test Vectors

Table 20 presents two test vectors for Orthros.

Table 20: Test vectors for Orthros in hex.

Plaintext	00000000000000000000000000000000
Key	00000000000000000000000000000000
Ciphertext	6060acb118f411e434ba4e01984de0de
Plaintext	a947436710924ccd47f2d571deea8f05
Key	4a2be60e3db6abe0c03eaec66fd05d0c
Ciphertext	e4cec0d077a3401d8c4d07b6d5196e5f